possible topics

interaction of airflow w/ mtns

- Kelvin waves
- trapped density currents
- barrier jet
- bores
- mesoscale eddies e.g.
  - Catalina eddy
  - Denver conv.-vert. zone
  - Longmont antecyclone
- mountain waves
  - downslope windstorms
  - ⋮

→ precip. * orography

← SI & CSI

- HCRs
- sea-breeze front, mt.-valley circ.
- MCSs

METR 6413

Advanced Mesoscale Meteorology

Emanuel (1984) Mesoscale Meteor. & Forecasting

mesoscale

observations

dynamics

history

Ligda (1951) radar obs. — unlike synoptic-using sfc obs, rawinsonde obs

smaller than synoptic

"not" observed with contemporary obs. systems

Is mesoscale part of a continuum?

Is mesoscale related to ordered processes → generate KE on "mesoscale"

dynamics —

normal modes of oscillation?

buoyancy

vertical shear

f

Lagrangian time scale

$$\tau = \frac{L}{U}$$

$\frac{1000\,km}{10\,ms^{-1}} = 10^5\,s$ day

$\frac{100\,km}{10\,ms^{-1}} = \frac{10^5\,m}{10\,ms^{-1}} = 10^4\,s$ hrs

$\frac{1\,km}{100\,ms^{-1}}$ ~~$= \frac{10^3\,m}{100\,ms^{-1}} = 10\,s$~~ $\frac{10\,km}{10\,ms^{-1}} = 10^3\,s$ min

→ instabilities — convective grav. waves

→ forced mesoscale circ. — mt. waves

local intermittent

fronts — hybrid

$\tau = \frac{10\,km}{10\,ms^{-1}}$ no inertia, but, U slows down at front — semi-geostrophy

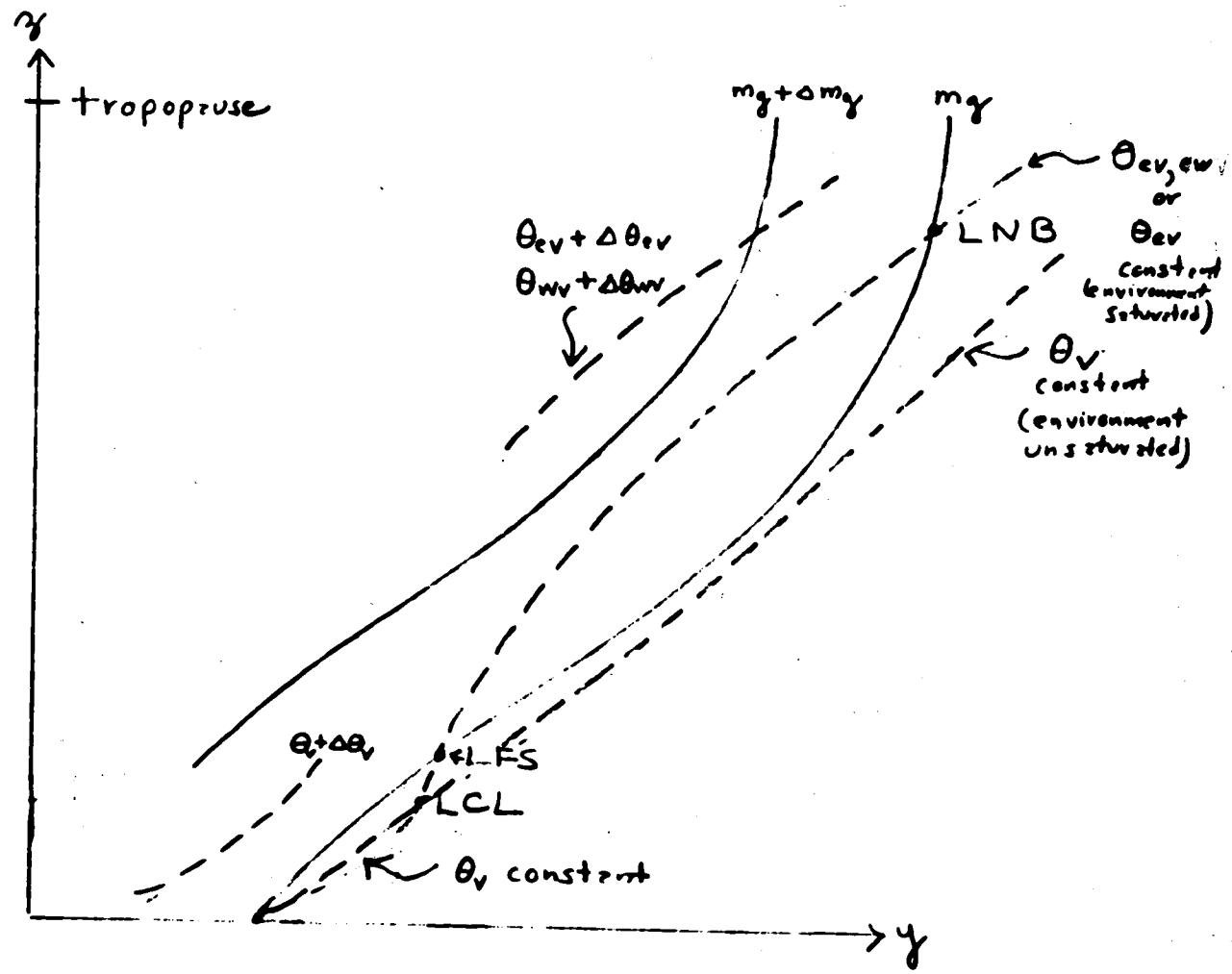

$\frac{\partial \theta_v}{\partial y} < 0$ baroclinic

$\frac{\partial \theta_v}{\partial z} > 0$ gravitational stability $\quad \frac{\partial \theta_{ev}}{\partial z}, \frac{\partial \theta_{wv}}{\partial z} > 0$ conditional stability

$\frac{\partial m_y}{\partial y} < 0$ inertial stability

- - - - - S surface

review pp 339–350, pp 545–561) vol. II

→ relevance to rainbands in extra cyclones hurricanes?

Conditional symmetric instability

parcel eqns.
$$\begin{cases} \dfrac{Dv}{Dt} = -f(m - m_g) \\ \dfrac{Dw}{Dt} = \dfrac{g}{\theta}(\theta' - \theta) \end{cases}$$
tube, env.; tube, env

$\frac{Dm}{Dt} = 0$

if env. moist, but unsat'd $\theta \to \theta_v$ $\qquad \theta' \to \theta'_v$

if env. sat'd. $\theta \to \theta_{ev}$ (θ_{wv}) $\qquad \theta' \to \theta'_{ev}$

~~if env. unsat'd~~ $\theta \to \theta_v$ $\qquad \theta' \to \theta'_{ev}$

define a sfc along which a tube is neutrally buoyant →

S sfc. (can include water loading, etc.)

$dm_g = \frac{\partial m_g}{\partial y} dy + \frac{\partial m_g}{\partial z} dz = 0$

$\left(\frac{-z}{\partial y}\right)_{m_g} = -\frac{\partial m_g/\partial y}{\partial m_g/\partial z} = \frac{-\partial \theta_v/\partial y + f}{\partial \theta_v/\partial z} \sim \frac{\partial T}{\partial y}$

show fig. & explain

LCL

LFS

LNB — in trop $\left|_{m_g \text{ vert.}}\right. \frac{\partial T}{\partial y} = 0$ $\quad$ θ being $\sim$ stray static stability

CSI — conditional symmetric instability

KE needed to lift tube to its LFS?

not needed

$$KE = \int_{y(z=0)}^{y(z=LFS)} f(m - m_g)\,(dy)_s$$

along neutral buoyancy sfc!

restoring force on tube

θ_{ev} or θ_v

$$\vec{F} = -f(m - m_g)\,\hat{j} + \frac{g}{\theta}(\theta' - \theta)\,\hat{k}$$

$m = u - fy$

$$\vec{\nabla} \times \vec{F} = \begin{vmatrix} \hat{i} & \hat{j} & \hat{k} \\ \frac{\partial}{\partial x} & \frac{\partial}{\partial y} & \frac{\partial}{\partial z} \\ 0 & -f(m - m_g) & \frac{g}{\theta}(\theta' - \theta) \end{vmatrix} = \hat{i}\left[\frac{\partial}{\partial y}\frac{g}{\theta}(\theta' - \theta) + \frac{\partial}{\partial z} f(m - m_g)\right] = 0$$

$-f\frac{\partial u_g}{\partial z} = \frac{g}{\theta}\frac{\partial \theta}{\partial y}$

$$-\hat{j}\left[\frac{\partial}{\partial x}\frac{g}{\theta}(\theta' - \theta)\right] - \hat{k}\frac{\partial}{\partial x} f(m - m_g)$$

$\frac{\partial}{\partial x} = 0$

$= 0 \Rightarrow$ $\vec{F}$ conservative, integral path indep.

define $\text{SCAPE} = -\int_{y(z=LFS)}^{y(z=LNB)} f(m-m_g)(dy)_s$ destroyed by SCAPE gain!

slantwise convective available potential energy

integral is path independent $\Rightarrow$

in general $\text{SCAPE} = -\int_{y(z=LFS)}^{y(z=LNB)} f(m-m_g)\,dy + \int_{z=LFS}^{z=LNB} \frac{g}{\theta_{ev}}(\theta_{ev}'-\theta_{ev})\,dz$

$$= \int_{z=LFS}^{z=LNB} \frac{g}{\theta_{ev}}(\theta_{ev}'-\theta_{ev})(dz)_{m_g} \quad \text{along } m_g \text{ sfc.}$$

$\longrightarrow$ note similarity to CAPE in parcel theory of convection!

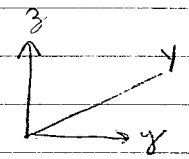

m_g sfc. parallel to Y coordinate

$\left(\frac{dz}{dy}\right)_{m_g} = \frac{S_y + f}{\frac{g}{\theta_{ev}}\frac{\partial\theta_{ev}}{\partial z}}$

SCAPE $\equiv$ CAPE in geos. coord.

barotropic $\Rightarrow$ m_g, Y vertical $\Rightarrow$ SCAPE = CAPE !

$\rightarrow$ ascertain the susceptibility of atm. to ordinary convection along an m_g sfc to ascertain susceptibility to slantwise convection

must analyze vertical cross section of m_g, T, T_d, θ_e, θ_{ev}

Show figs
- reg soundings
- X-sections
- Soundings along m_g sfc.

CHH ØZ 12/11/82

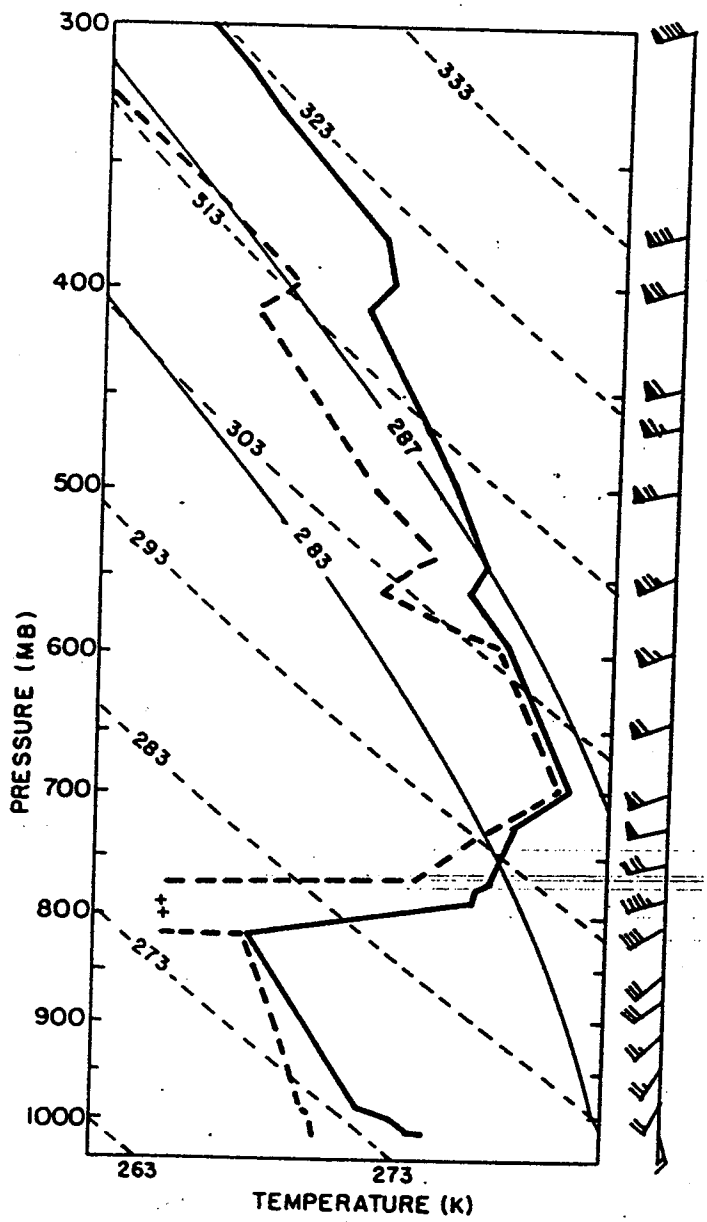

3.95

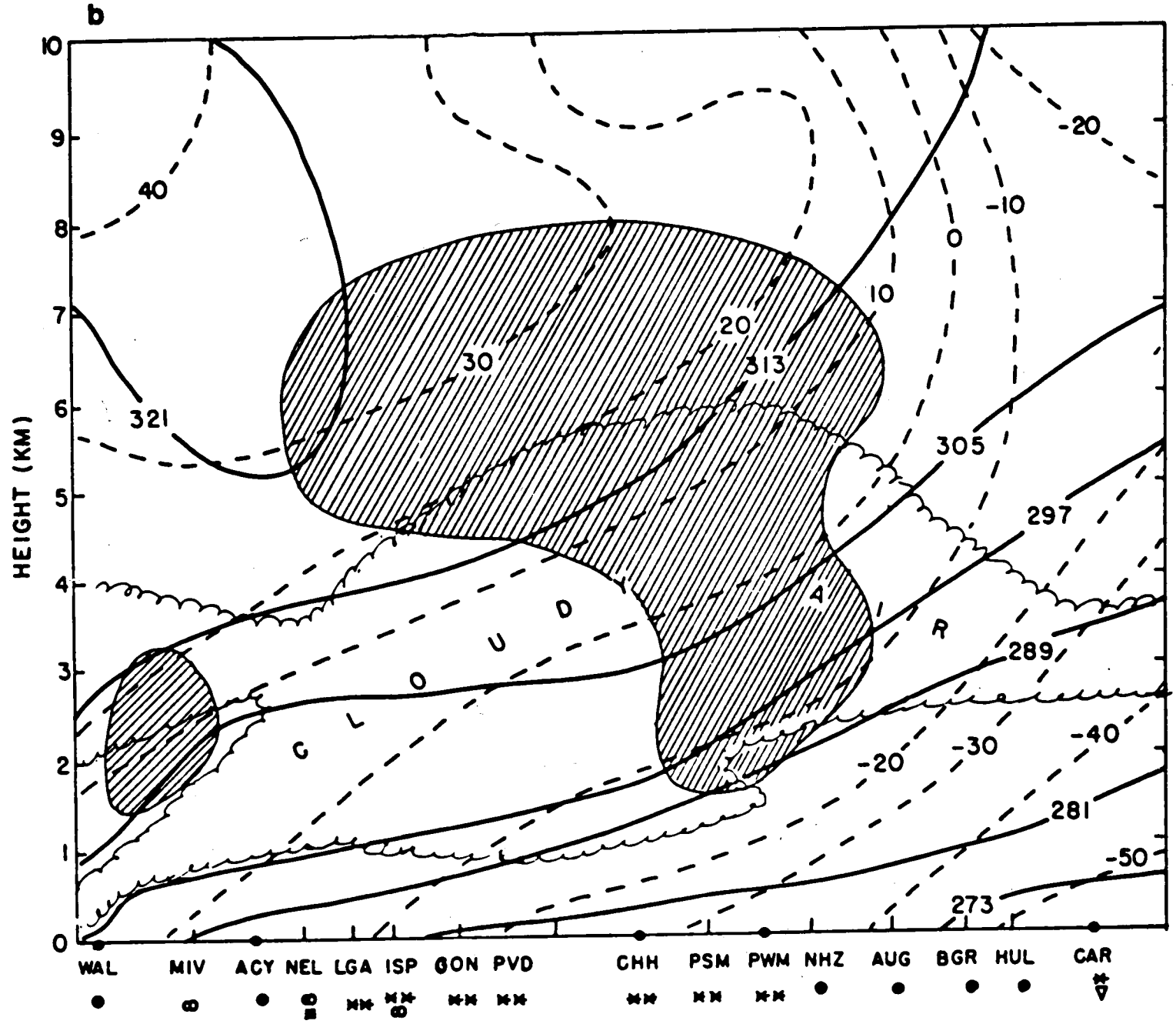

from Wolfsberg, et al. (1984)

FIG. 10. Vertical cross sections of θ_e in K (solid lines) and M_g in m s^{-1} (dashed lines) at (a) 00 GMT and (b) 12 GMT. Clouds are indicated with scalloped lines and regions of possible conditional symmetric instability are shaded. Upper air stations are indicated on the abscissa with large dots. Weather observed at surface stations is indicated below the axis (** = light snow, ∘∘ = light rain, ∇ = showers, ▬ = fog, ● = skies overcast, O = skies broken and ∞ = haze).

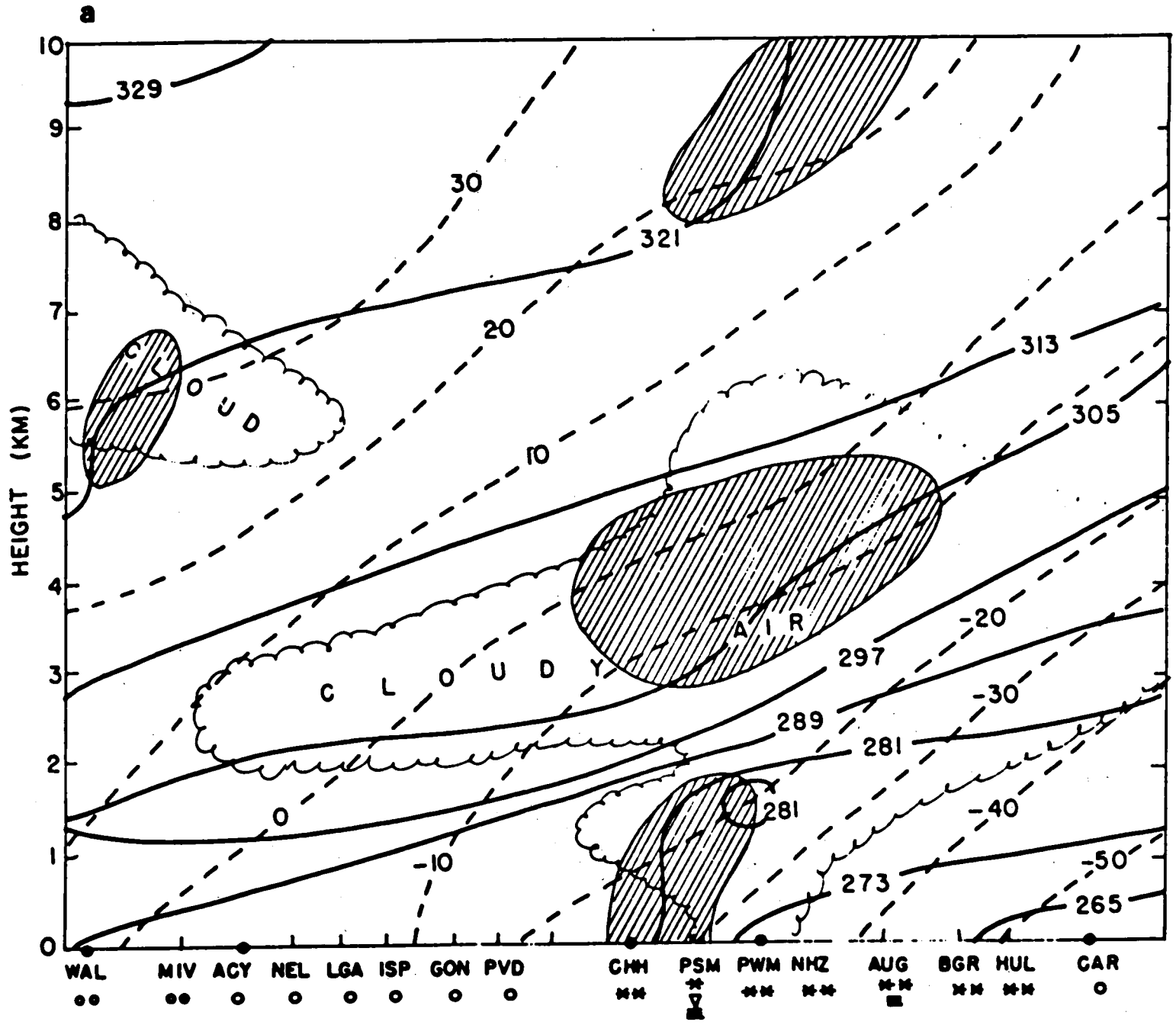

from Wolfsberg, et al (1972)

Sounding along $m_g = -10\ ms^{-1}$ sfc
at ϕZ 12/11/82

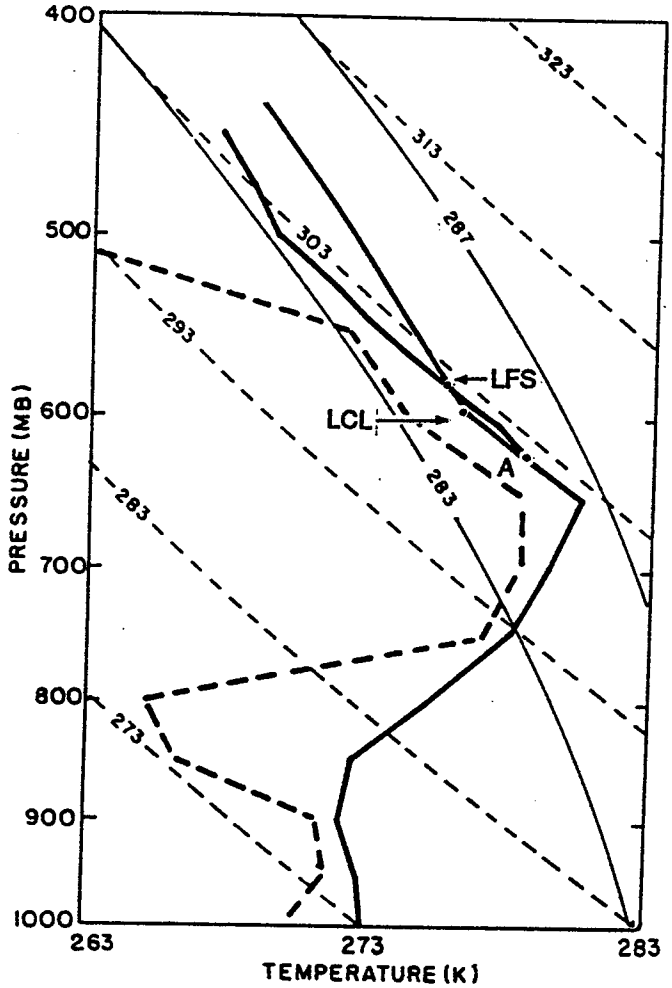

3.97

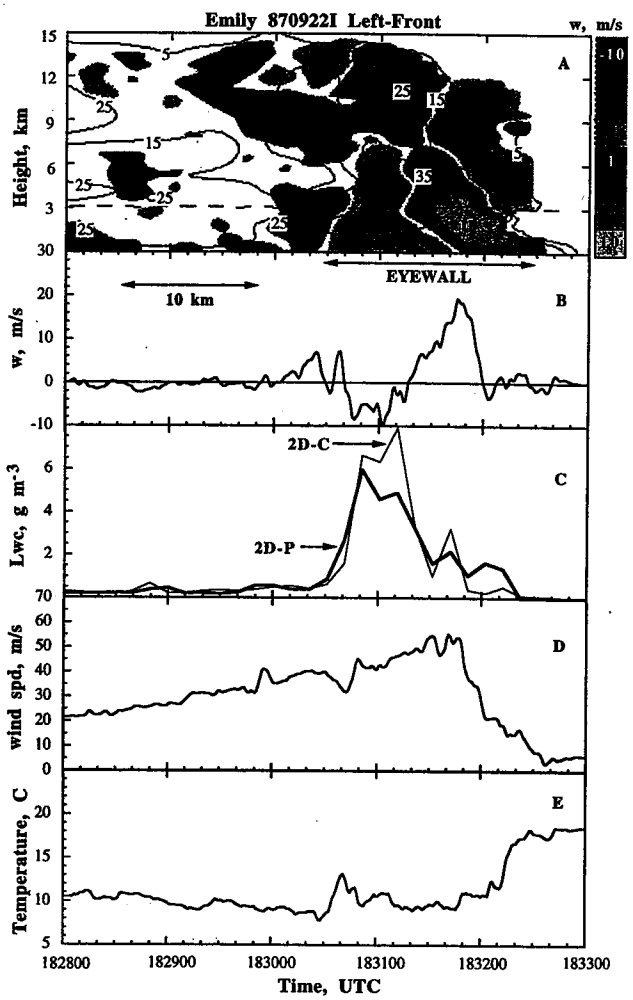

FIG. 4. Vertical cross section of (a) Doppler-derived vertical velocity and reflectivity (a as in Fig. 2), (b) plus flight-level vertical velocity, (c) precipitation water content, (d) horizontal wind speed, and (e) temperature for Doppler pass 9 in the left-front quadrant. The position of the Doppler aircraft is shown in (a) as the dashed line at approximately 3-km altitude.

strong downdrafts. The radially outward sloping downdraft contained moderate precipitation (Fig. 4c), whereas the inner downdraft (which was mostly above flight level) was barely represented in the flight-level vertical winds (Fig. 4b). The Doppler-derived vertical winds and the flight-level vertical winds match up well. A temperature increase (Fig. 4e) consistent with compressional warming marked the aircraft's entry into the broad outer downdraft. Downdraft zones that are wider near the surface (as in Fig. 4a) are not common in the hurricane eyewall. This may indicate that the downdraft air is diverging at the surface. The horizontal wind speed (Fig. 4d, at 1830:40) in the downdraft decreased slightly at the same time that a small relative maximum in temperature (Fig. 4e) occurred. We believe this decrease in wind speed was a result of vertical mixing with air having lower horizontal momentum above flight level. The outward slope of the reflectivity contours between the surface and 15 km in this portion of the eyewall is about 35° from the vertical, which is in accord with other observations (Jorgensen 1984b; Marks et al. 1992).

Another example of a strong downdraft in the left-front quadrant is shown for a radial pass in approximately the same portion of the eyewall as in Fig. 4 but for 2 h later (Fig. 5). This time the downdraft at 2032:30 was 9 km deep and had a maximum flight-level speed of approximately -8 m s^{-1}. The Doppler-derived vertical velocity field indicated that the strongest part of this downdraft was near 5 km. The 3-km flight-level data (Figs. 5b–e) showed that the highest precipitation liquid water content on both probes occurred near the RMW in the strong updraft, not in the downdraft as in Fig. 4. This updraft had the strongest vertical velocity observed at this level. A temperature

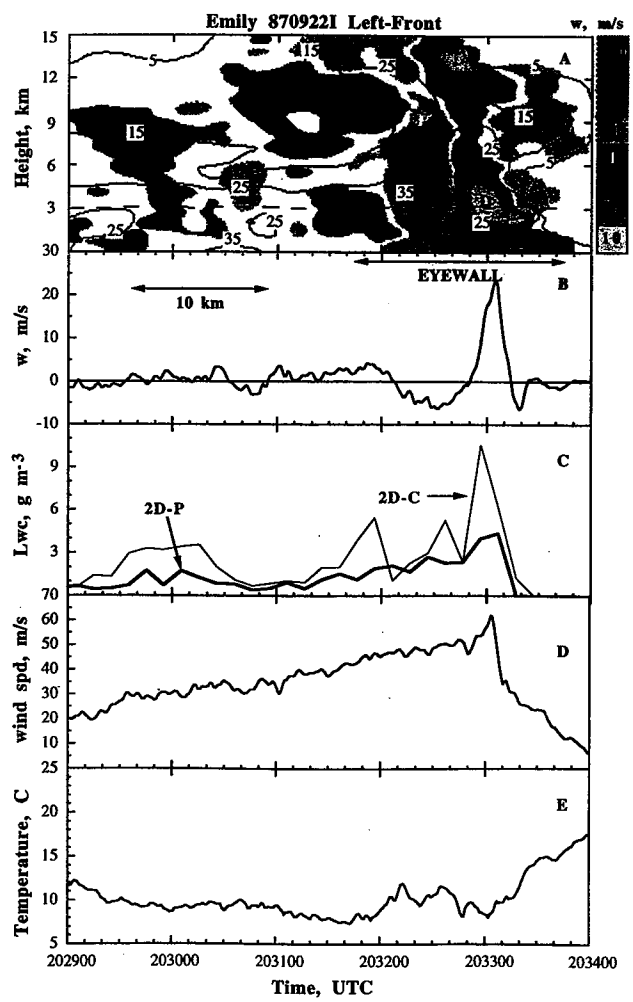

FIG. 5. As in Fig. 4 but for Doppler pass 13 in the left-front quadrant.

Bob Black, Blustein & Michael Black MWR Dec. 1994

$$\frac{Du}{Dt} = \frac{v^2}{r} + fv - \frac{1}{\rho}\frac{\partial p}{\partial r}$$

$$\frac{Dv}{Dt} = -\frac{uv}{r} - fu$$

$$\frac{Dw}{Dt} = g\left(\frac{\theta_e' - \theta_e}{\theta_e}\right)$$

$$M = r\left(v + \frac{fr}{2}\right) \longrightarrow \frac{DM}{Dt} = 0$$

$$\frac{Du}{Dt} = \frac{(M - M_{gr})(M + M_{gr})}{r^3}$$

in gradient wind balance

$$\frac{\partial M}{\partial r} > 0 \quad \text{inertial stability}$$

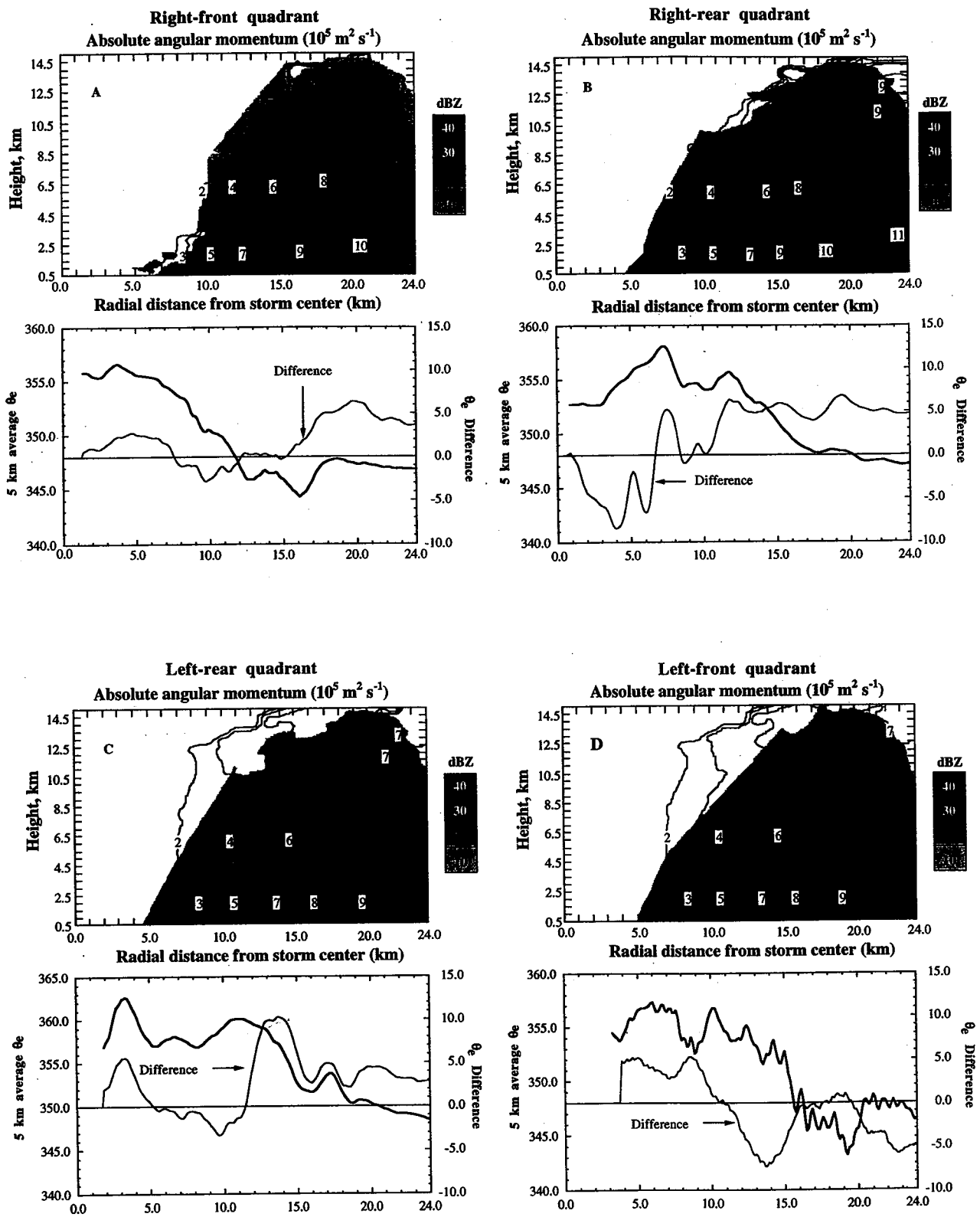

FIG. 17. Vertical cross sections of M (10^5 m^2 s^{-1}) in Hurricane Emily in the following quadrants: (a) right front, (b) right rear, (c) left rear, and (d) left front. Composites are valid for 1538–1744 UTC 22 September 1987. Average radar reflectivity in the range 10–40 dBZ is superimposed on the M plot. The mean quadrant θ_e from the H aircraft, and the θ_e difference H − I (i.e., the difference between θ_e at the higher level and θ_e at the lower level) are plotted. These data have been smoothed with a nine-point Gaussian filter for clarity.

uel
:nd
nu-
to
her
e's
lly
the
nd
ive
in-
act
'9)
as
ith
or-
ce.
ter
ac-
As
ess
el-
lly
ant
ted

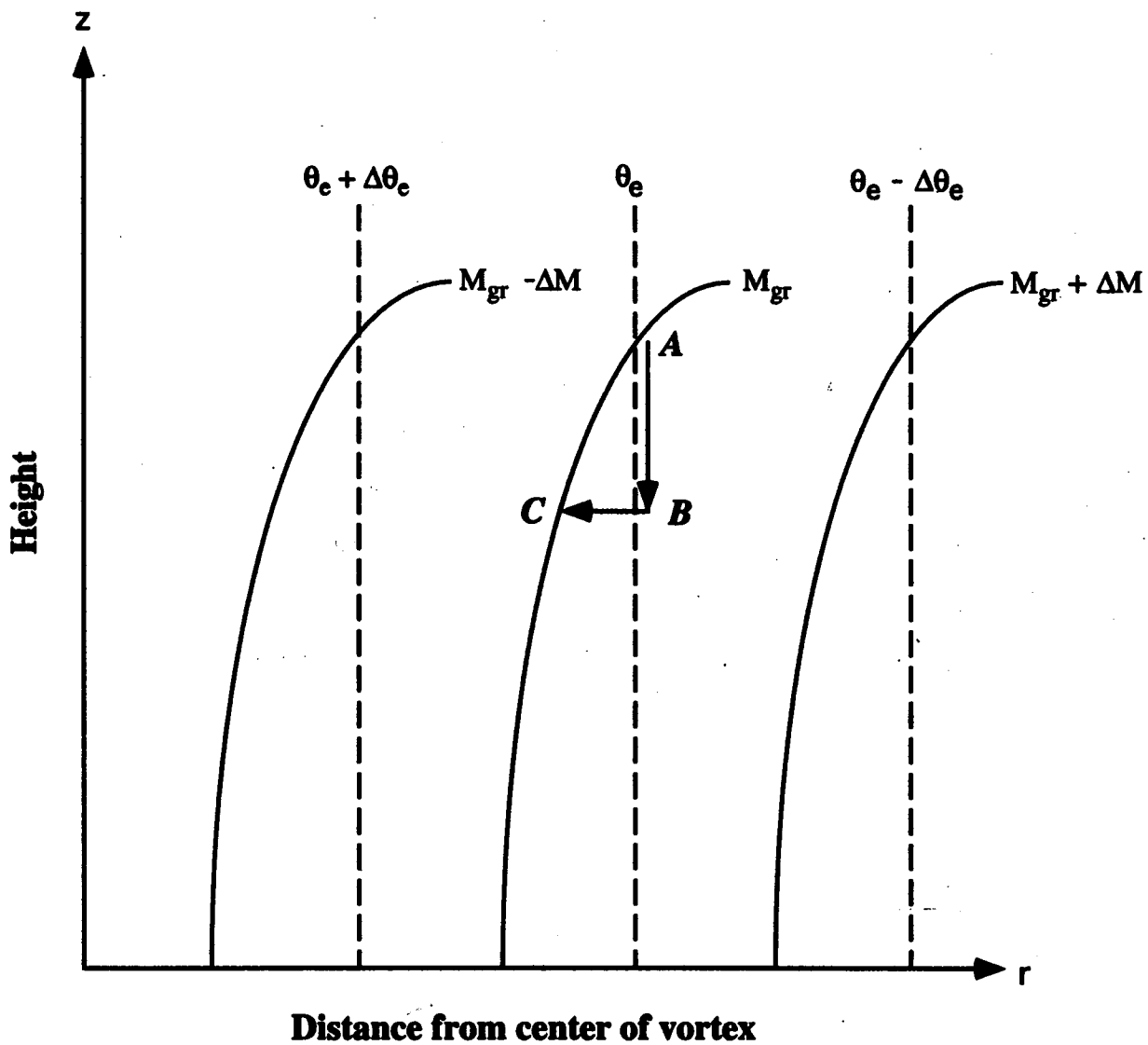

FIG. 16. Idealized vertical cross section of absolute angular momentum M (solid contours) and equivalent potential temperature θ_e (dashed contours) in the eyewall of a hurricane, above the boundary layer and below the tropopause. Here M_{gr} denotes the M of a vortex in gradient wind balance.

the storm-relative mean azimuthal wind component was
the determined. There are some regions aloft that appear
on to be inertially unstable ($\partial M/\partial r < 0$). However, the

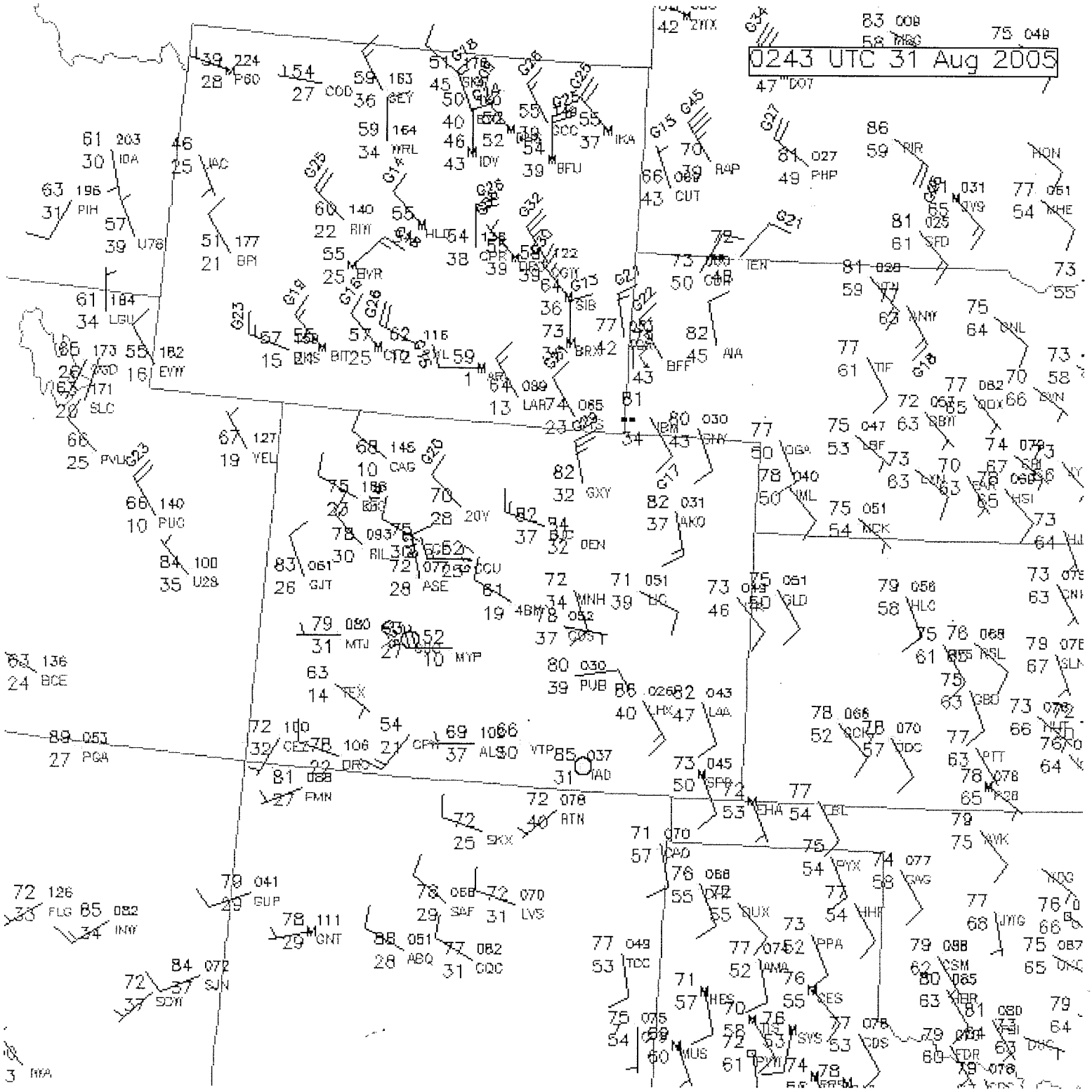
0243 UTC 31 Aug 2005

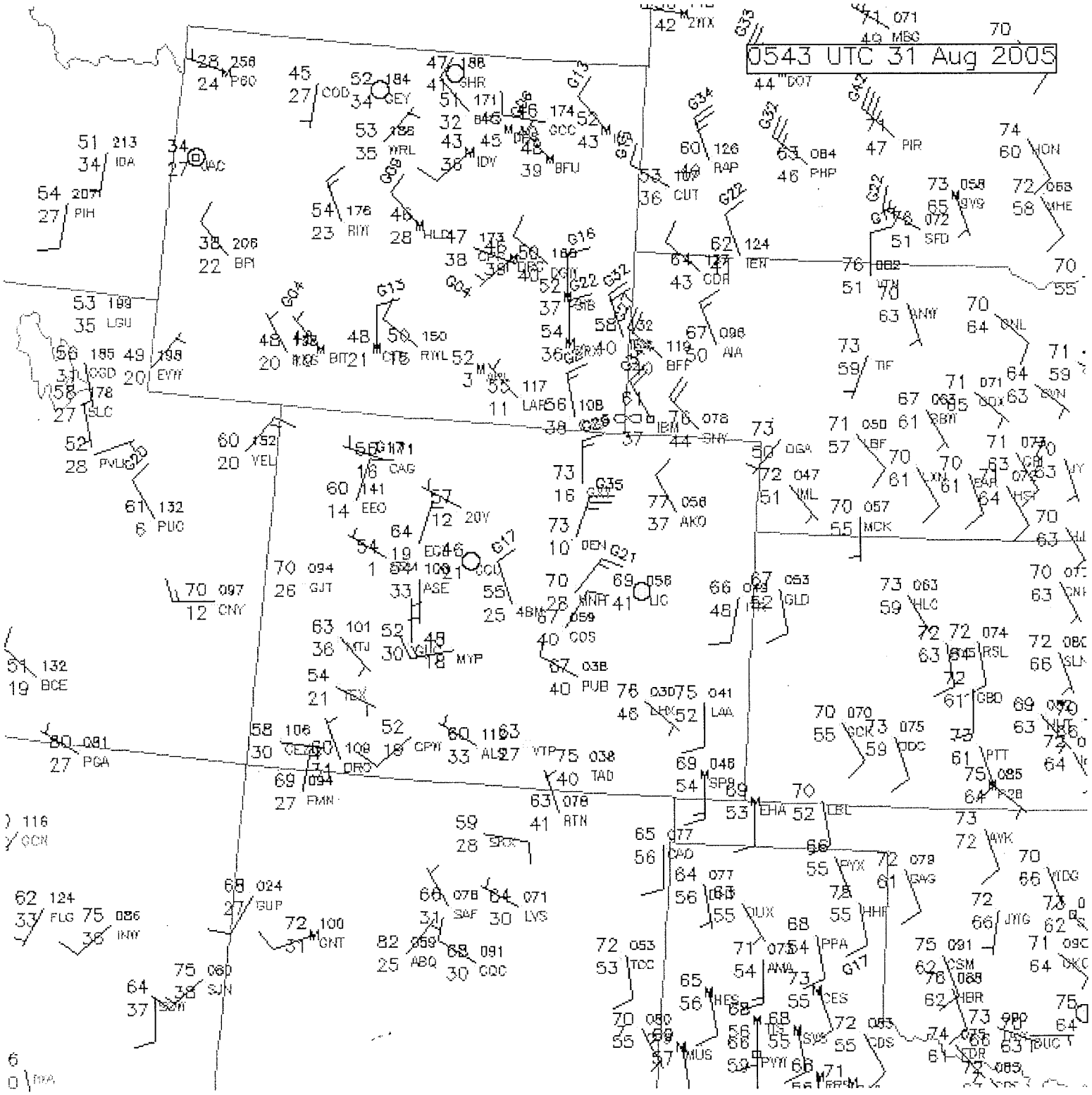
0543 UTC 31 Aug 2005

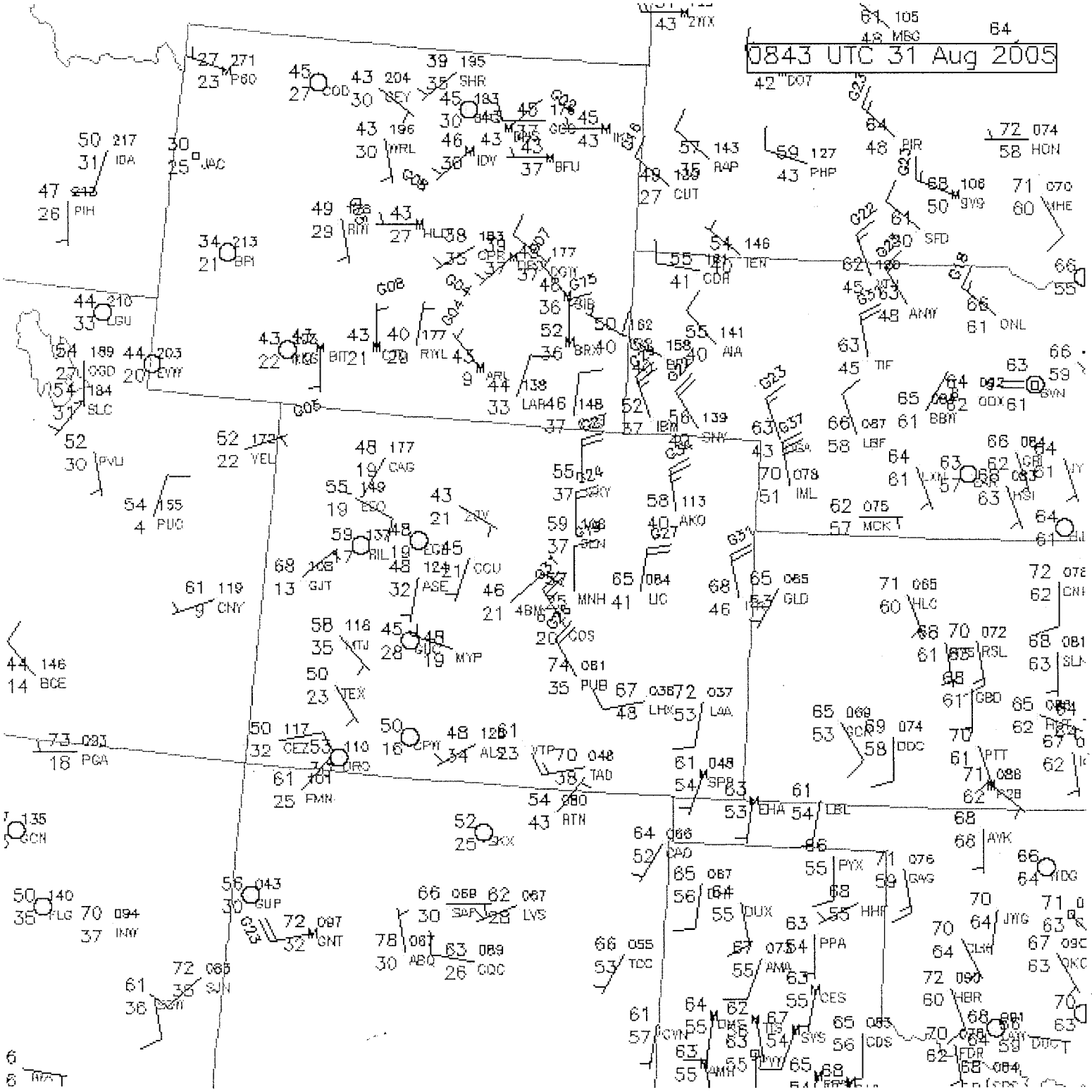
0843 UTC 31 Aug 2005

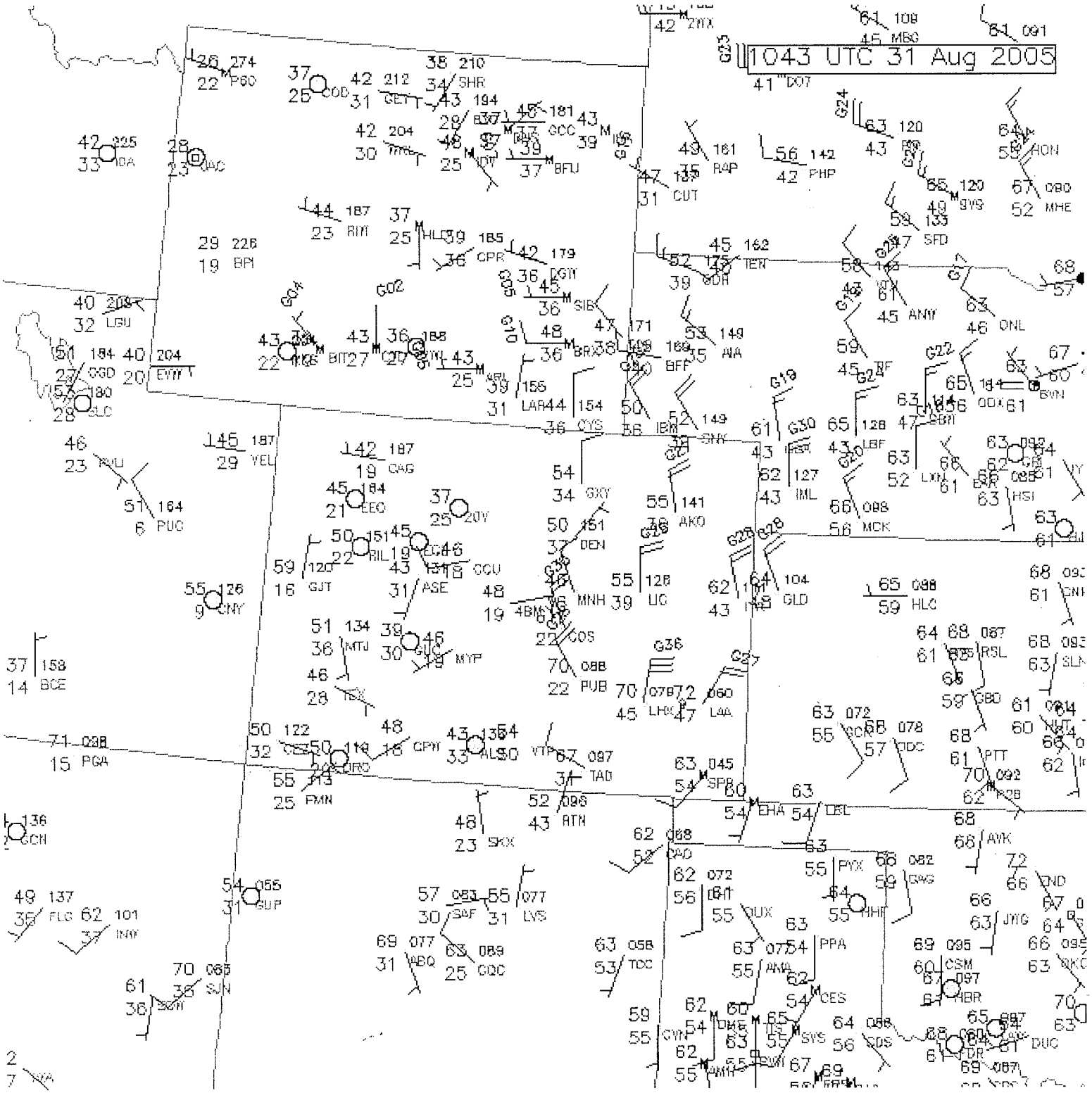
1043 UTC 31 Aug 2005

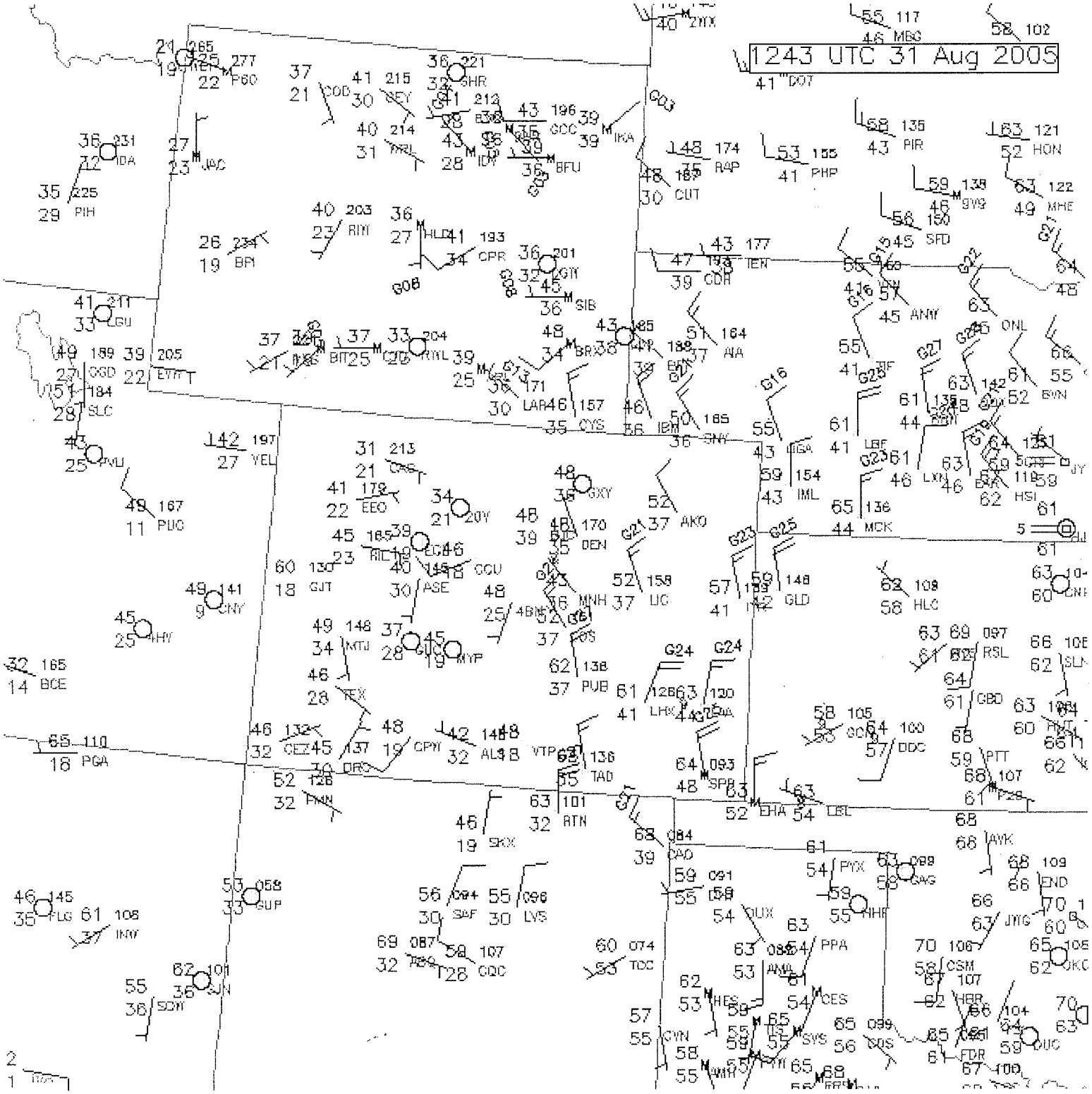
1243 UTC 31 Aug 2005

T(F)	Td	LI	SWT	K	TT	Pw(cm)	CAPE	Tc	CELL	SREH	VGP
53	38	9.0	70	3	31	1.29	0	87	308/20	64	0.00

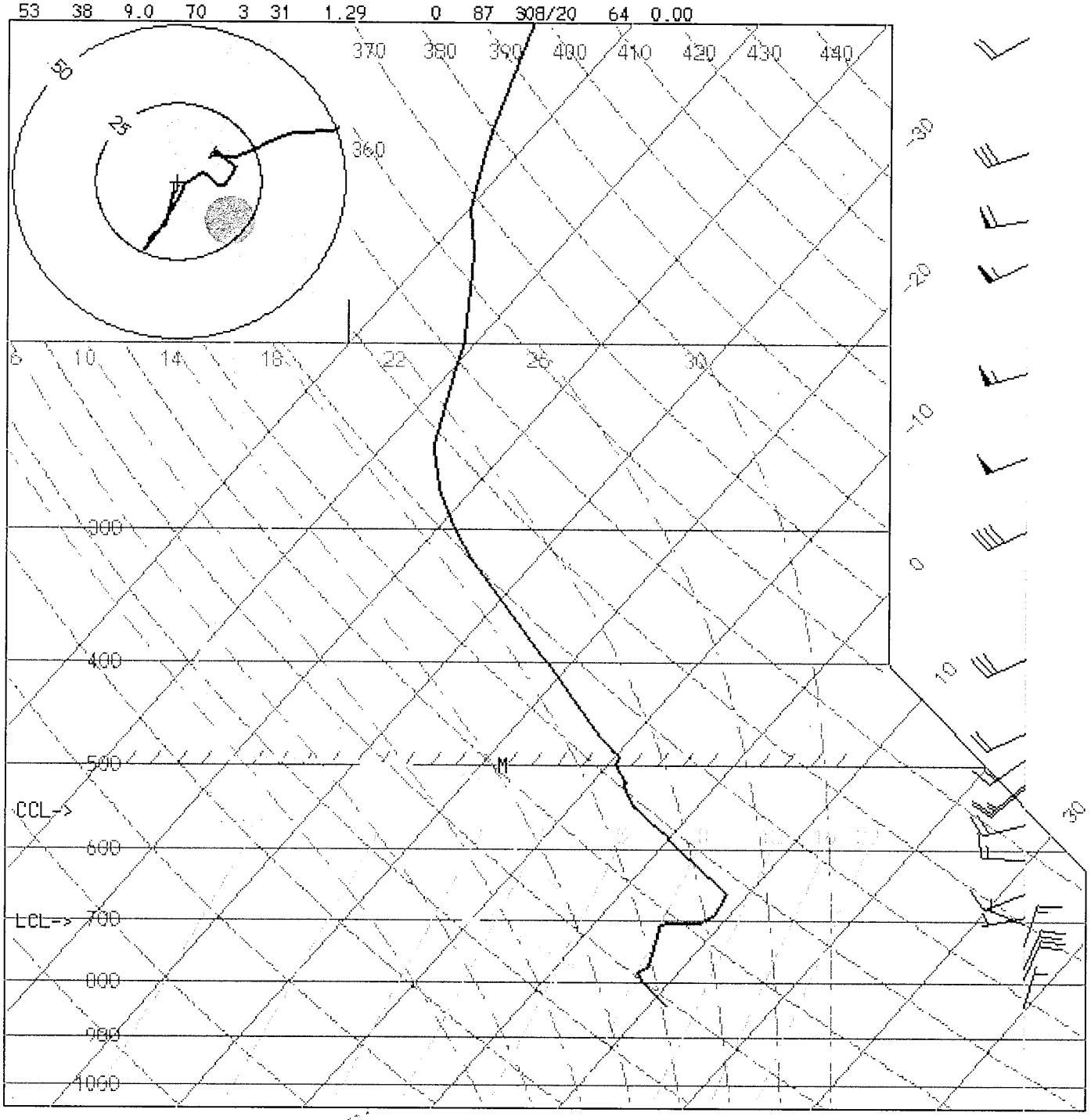

SKEW-T/LOG-P VALID 1200 UTC 08/31/2005 KDNR Lat = 39.75 , Lon = -104.87

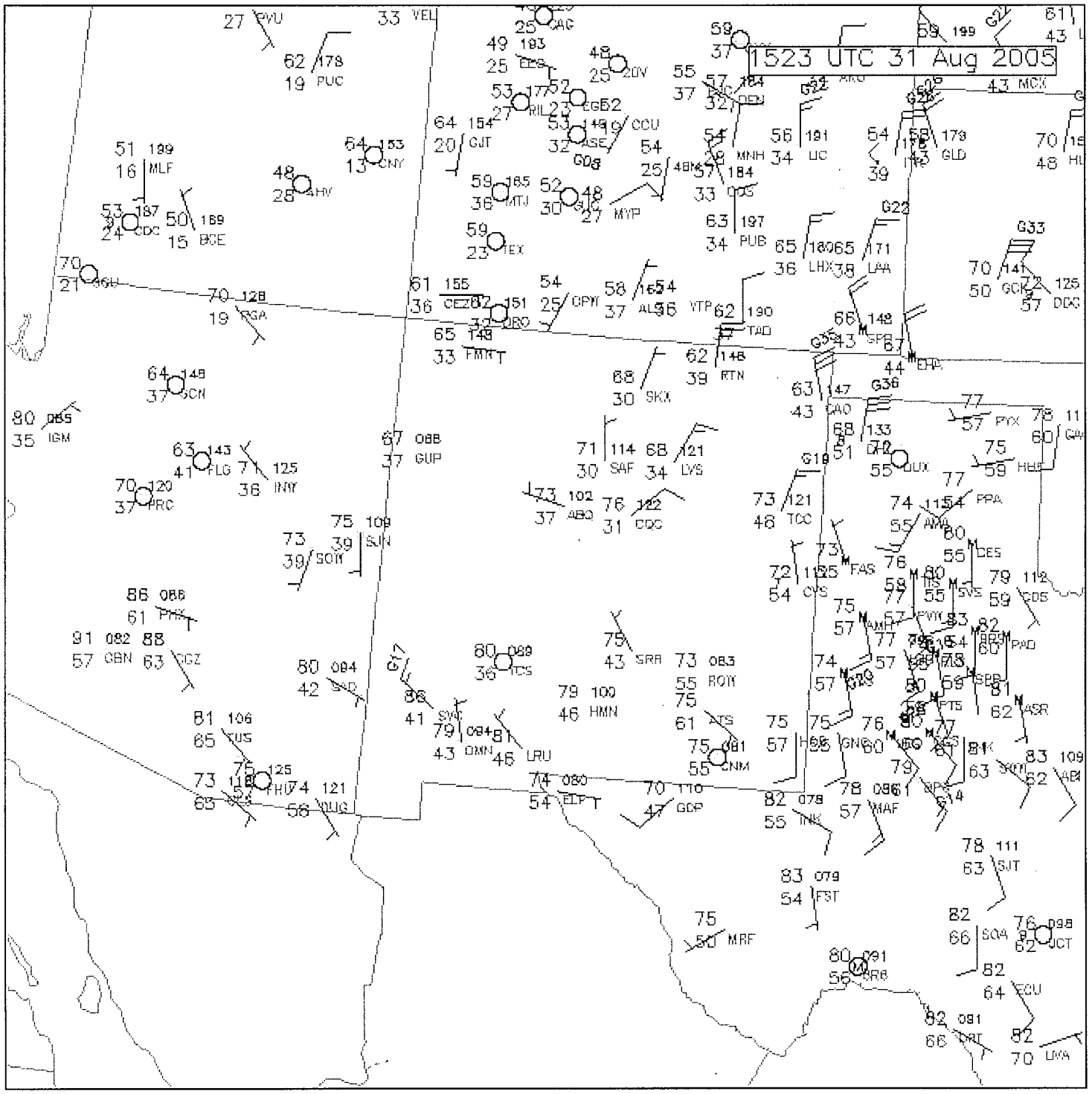

Page generated from http://www.rap.ucar.edu/weather/surface/ at Wed, 31 Aug 2005 15:24:33 GMT.

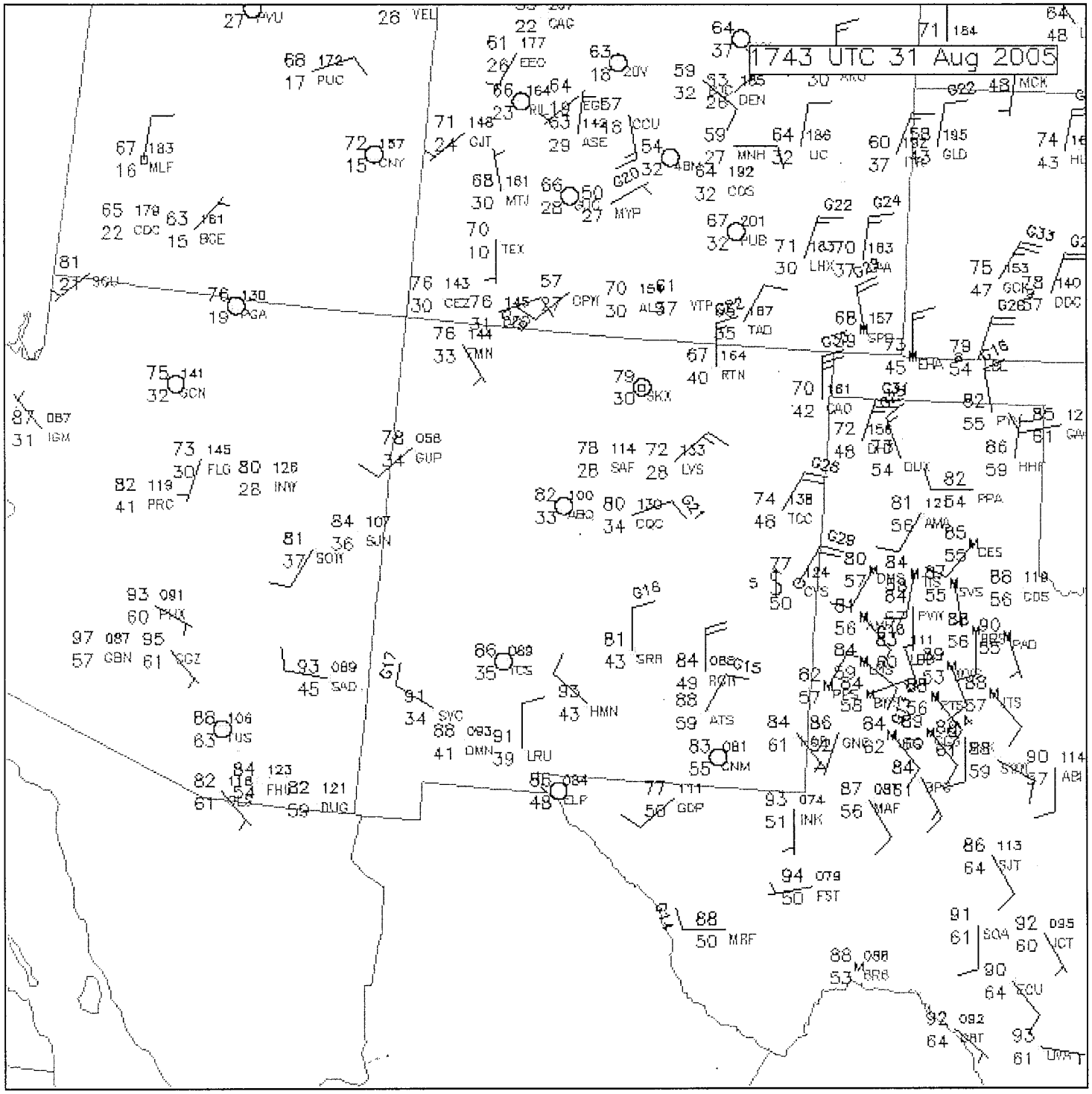

Page generated from http://www.rap.ucar.edu/weather/surface/ at Wed, 31 Aug 2005 17:47:08 GMT.

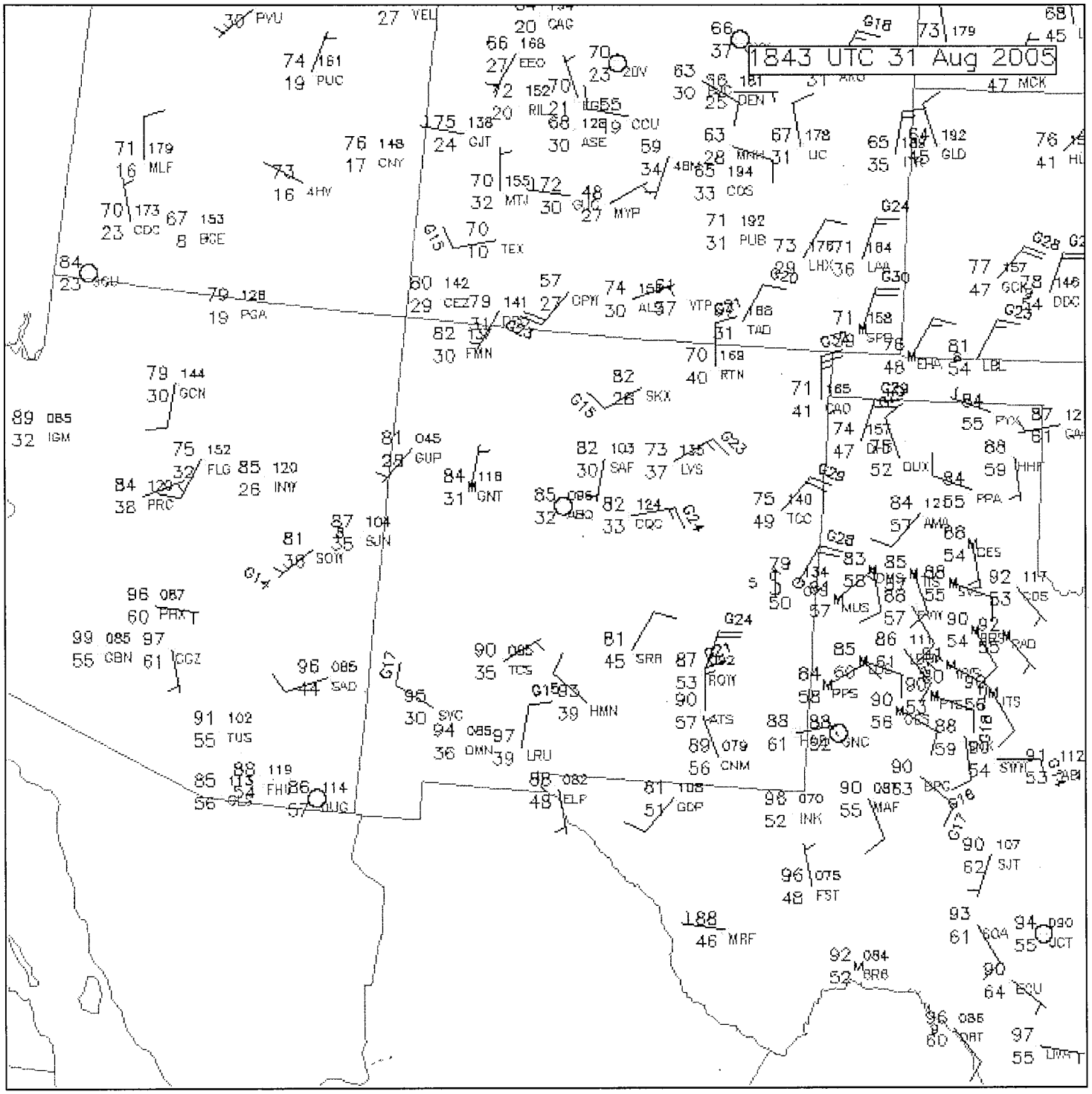

Page generated from http://www.rap.ucar.edu/weather/surface/ at Wed, 31 Aug 2005 18:53:06 GMT.

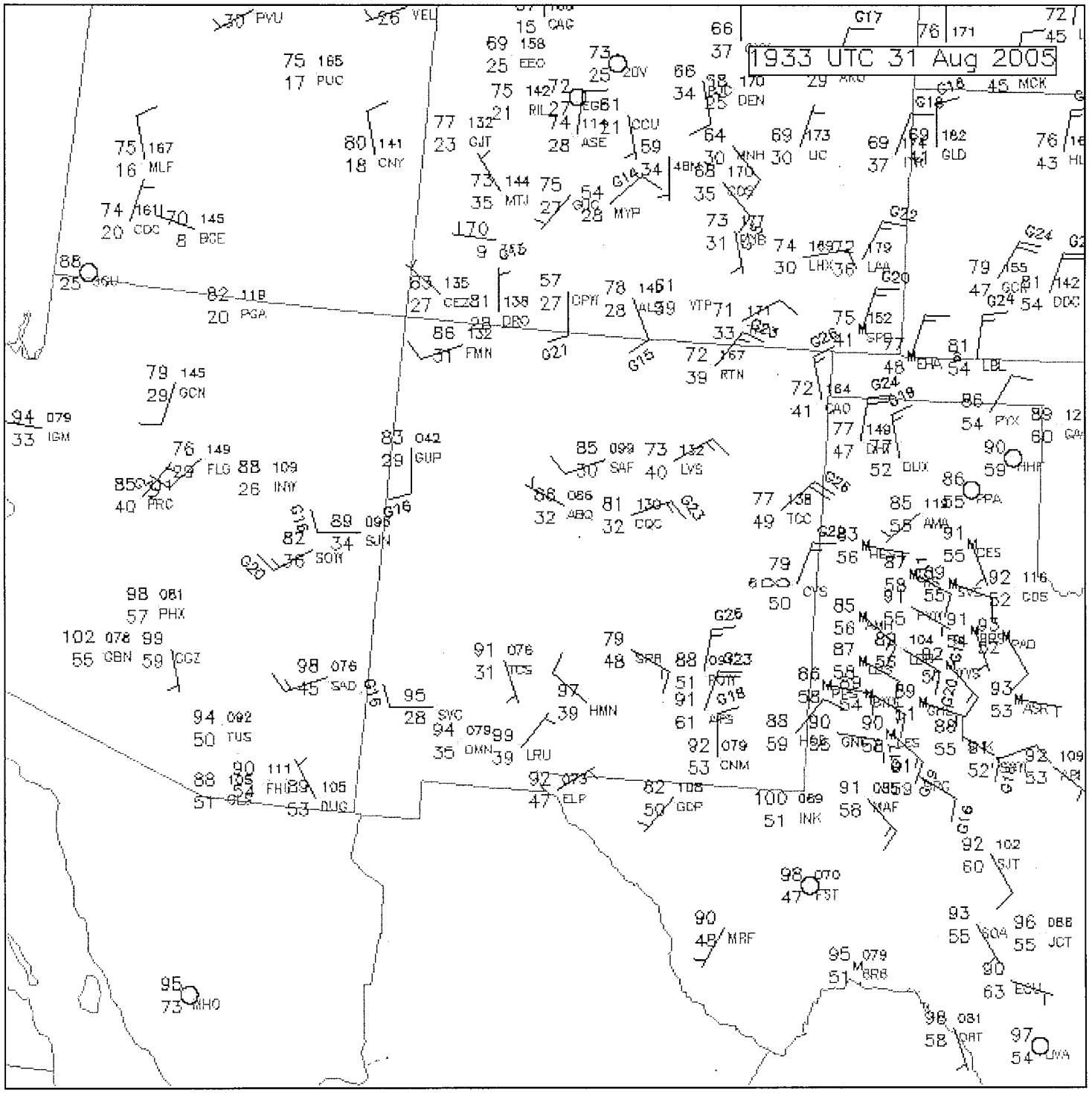

Page generated from http://www.rap.ucar.edu/weather/surface/ at Wed, 31 Aug 2005 19:34:38 GMT.

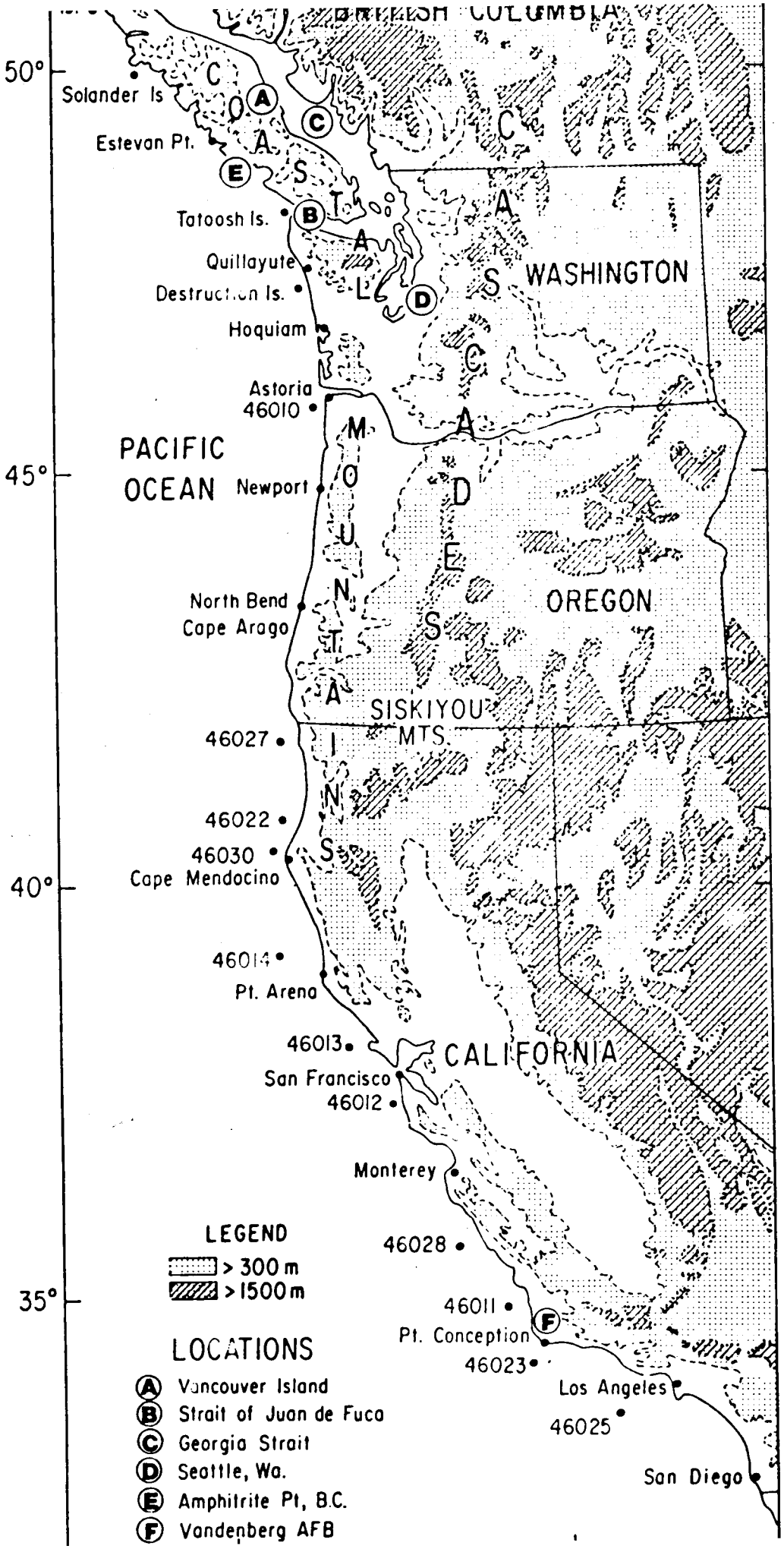
BRITISH COLUMBIA
50°
45°
40°
35°
Solander Is
Estevan Pt.
Tatoosh Is.
Quillayute
Destruction Is.
Hoquiam
Astoria
46010
PACIFIC
OCEAN
Newport
North Bend
Cape Arago
46027
46022
46030
Cape Mendocino
46014
Pt. Arena
46013
San Francisco
46012
Monterey
46028
46011
Pt. Conception
46023
Los Angeles
46025
San Diego
COAST RANGES
CASCADES
WASHINGTON
OREGON
SISKIYOU
MTS.
CALIFORNIA
LEGEND
> 300 m
> 1500 m
LOCATIONS
A Vancouver Island
B Strait of Juan de Fuca
C Georgia Strait
D Seattle, Wa.
E Amphitrite Pt, B.C.
F Vandenberg AFB

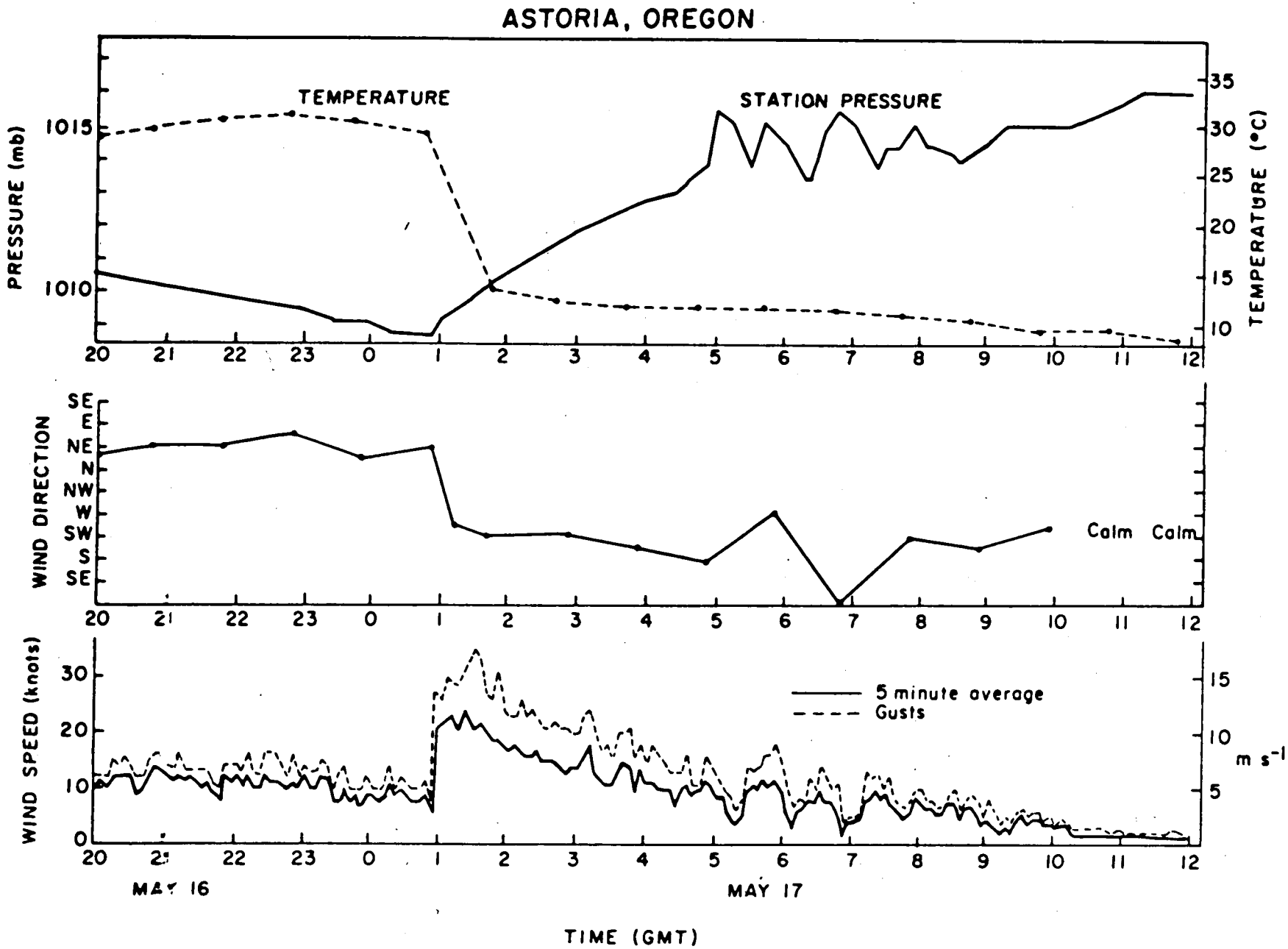

FIG. 2. Temperature, station pressure and winds at Astoria, Oregon from 20 UTC 16 May through 12 UTC 17 May 1985. Temperature and wind direction are based on hourly observations; station pressure and wind speed are from continuous recorders.

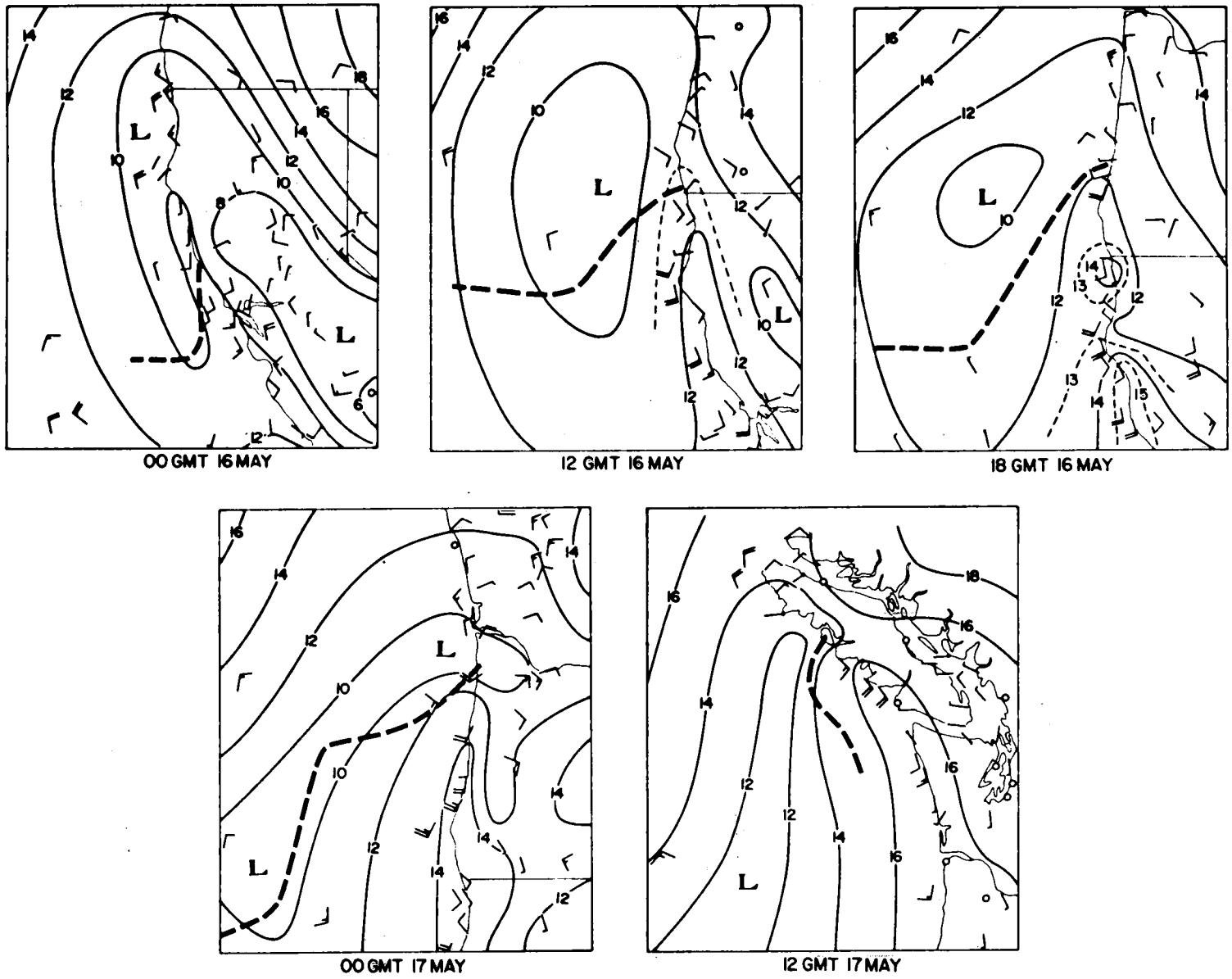

FIG. 10. Mesoscale sea level pressure analyses and surface winds in the immediate area surrounding the coastal surge for 12 UTC 15 May through 18 UTC 17 May 1985.

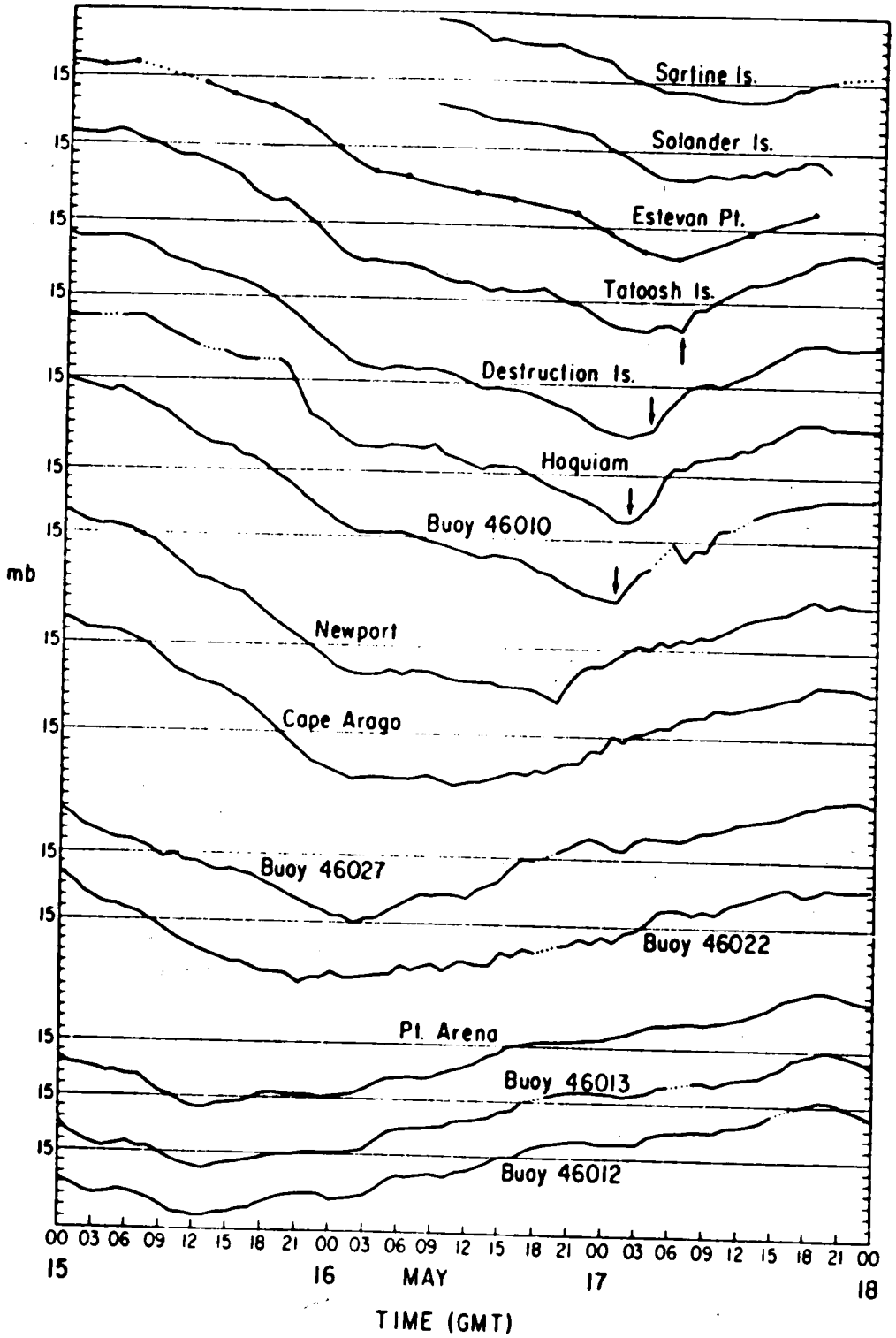

FIG. 12. Evolution of sea level pressure for a collection of coastal stations from central California to British Columbia for 00 UTC 15 May through 00 UTC 18 May based on hourly observations. Large solid dots indicate three hourly observations while dotted lines indicate periods in which an observation is missing. The vertical arrows indicate times of surge passage. Each pressure plot is relative to one of the horizontal 1015 mb lines. The tick marks indicate 1 mb intervals. The spacing of the traces is proportional to the distance along the coast between the observing sites.

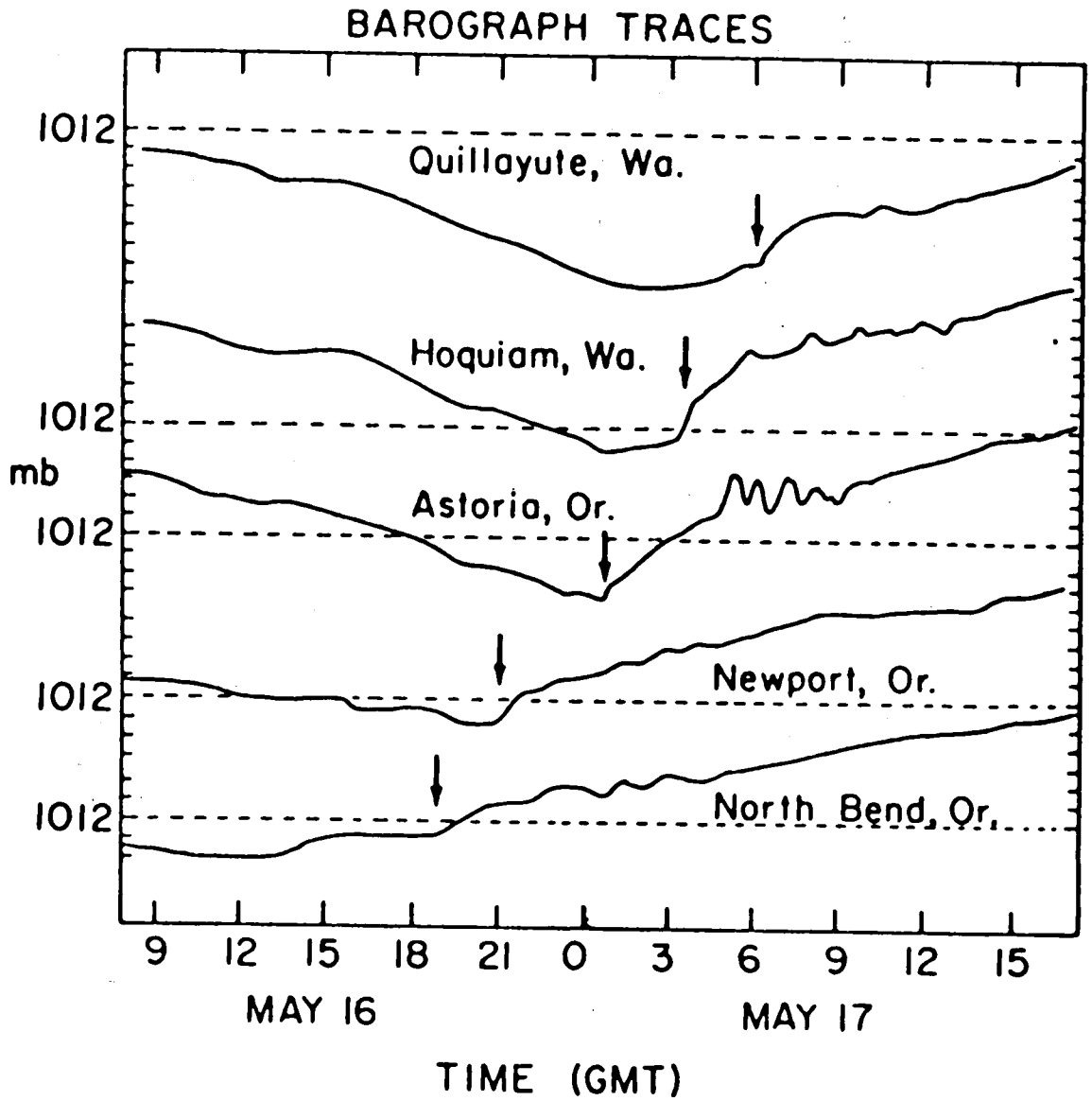

FIG. 13. Microbarograph traces at North Bend, Newport, and Astoria, OR, and Hoquiam and Quillayute, WA from 08 UTC 16 May through 18 UTC 17 May 1985. The vertical arrows indicate times of surge passage. The dashed horizontal axes represent 1012 mb and the tick marks indicate 1 mb intervals.

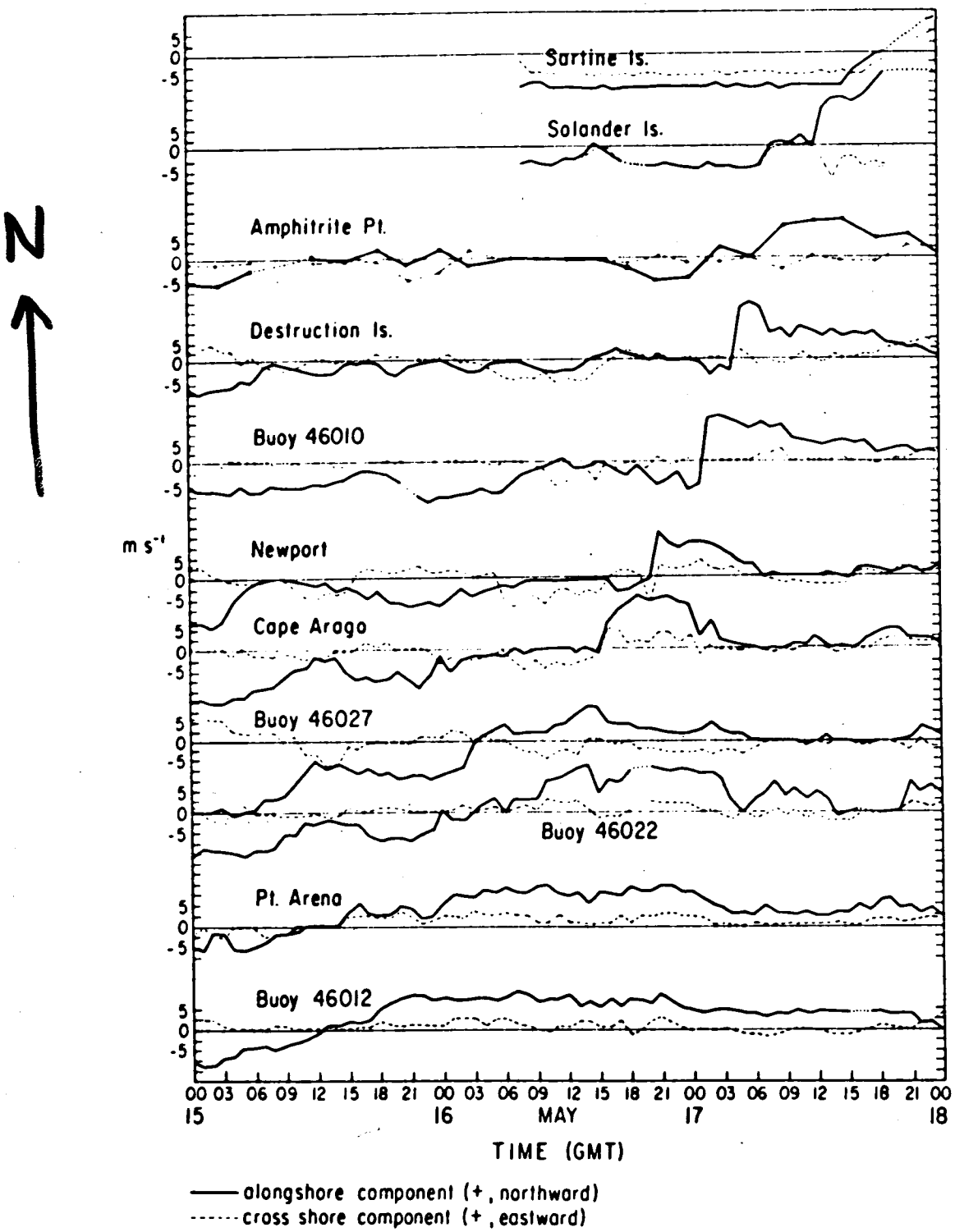

FIG. 15. Time evolution based on hourly observations of the alongshore and cross shore surface wind components for a series of coastal stations. Solid dots indicate three hourly observations and dotted lines indicate missing data. Tick marks represent 5 kt (2.5 m s^{-1}) intervals. The station spacing is approximately proportional to the distance along the coast.

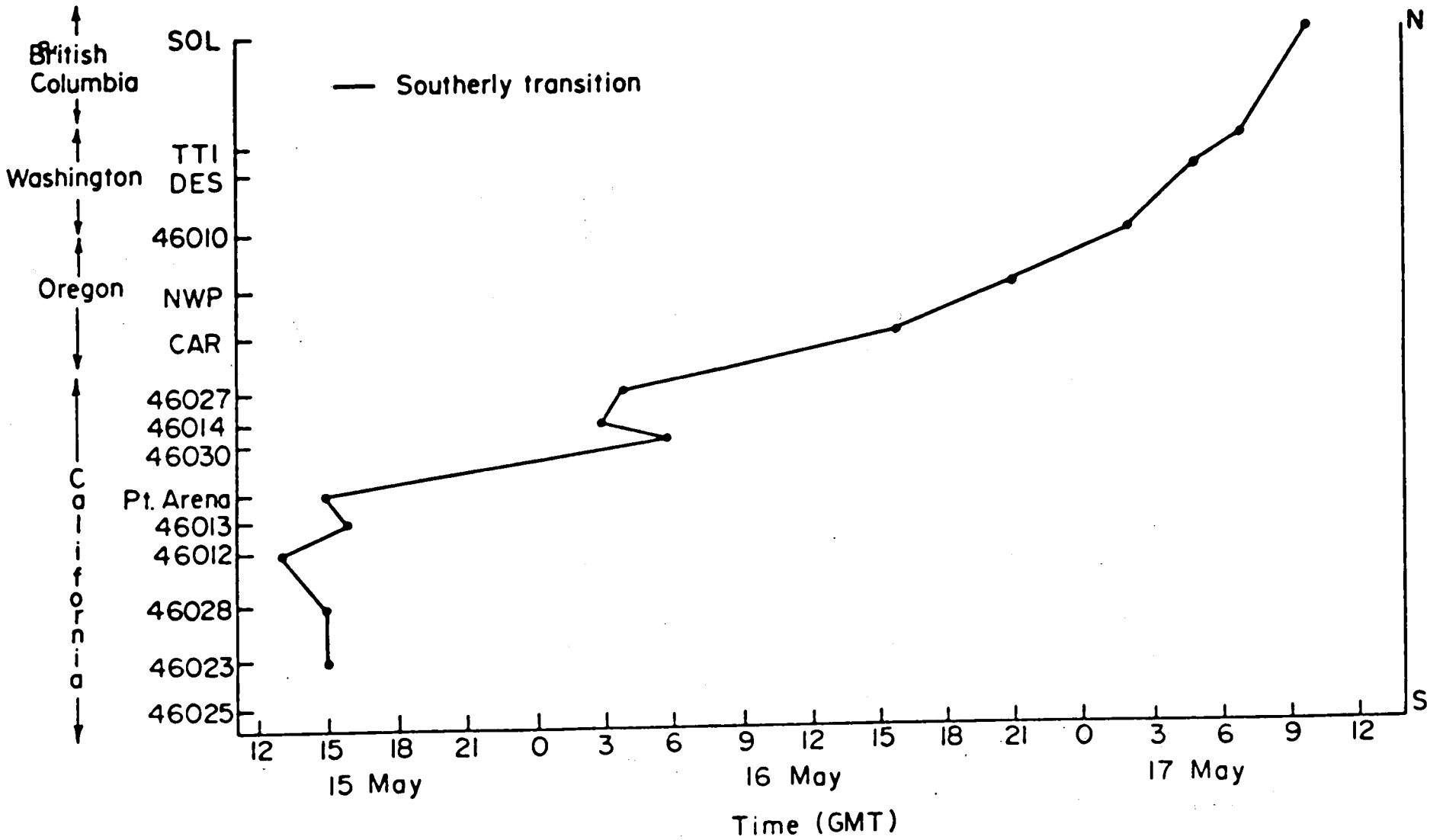

FIG. 16. Positions of the southerly transitions as a function of time.

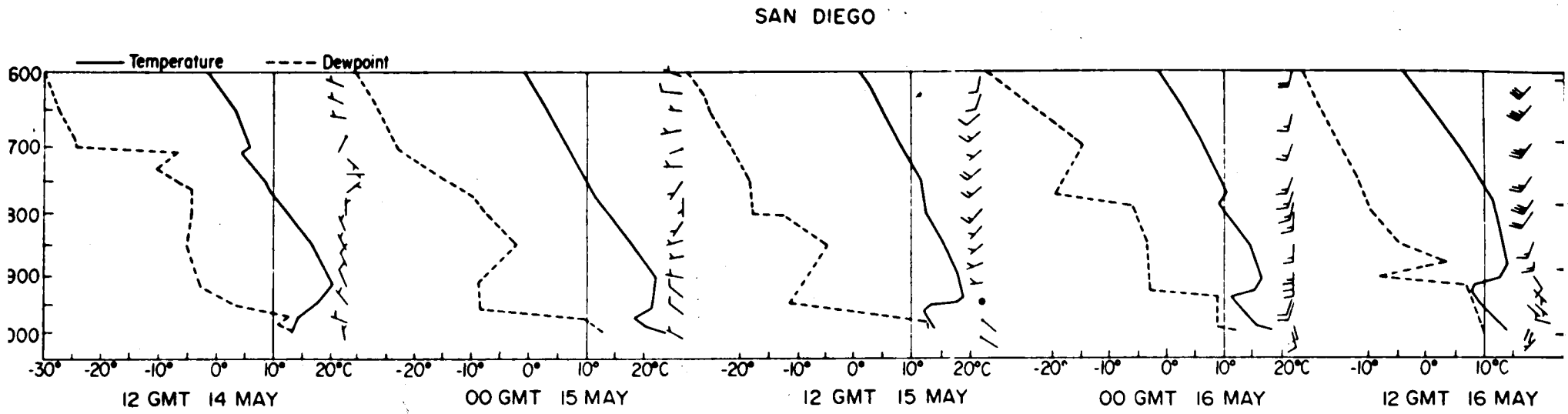

FIG. 18. Vertical soundings at San Diego, California from 12 UTC 14 May through 12 UTC 16 May 1985. Winds (knots) are plotted to the right of the corresponding temperature sounding.

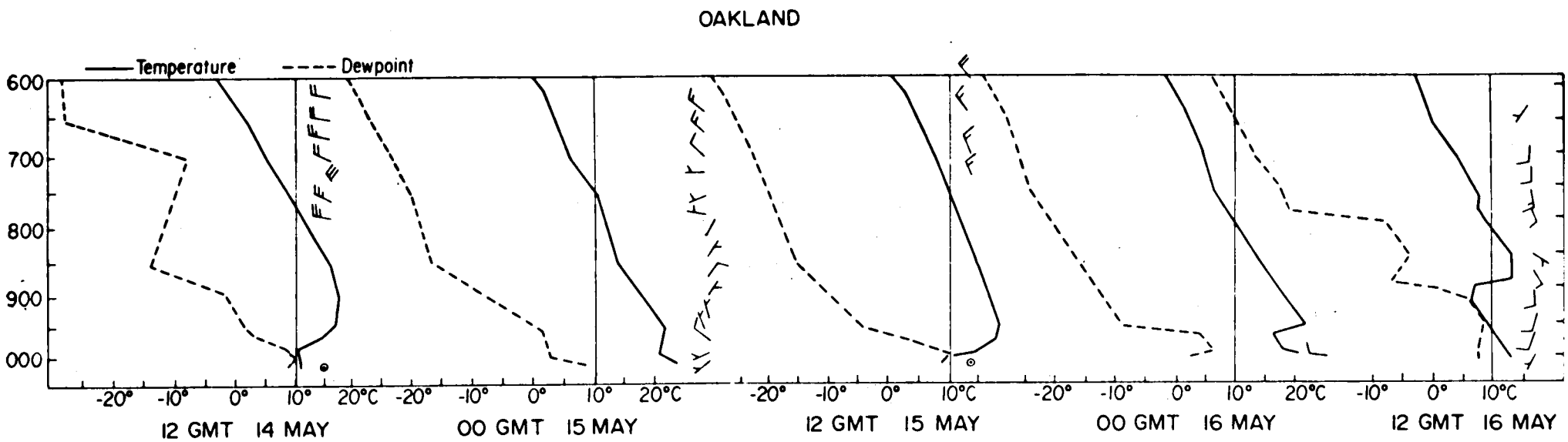

FIG. 19. Vertical soundings at Oakland, CA from 12 UTC 14 May through 12 UTC 16 May 1985.

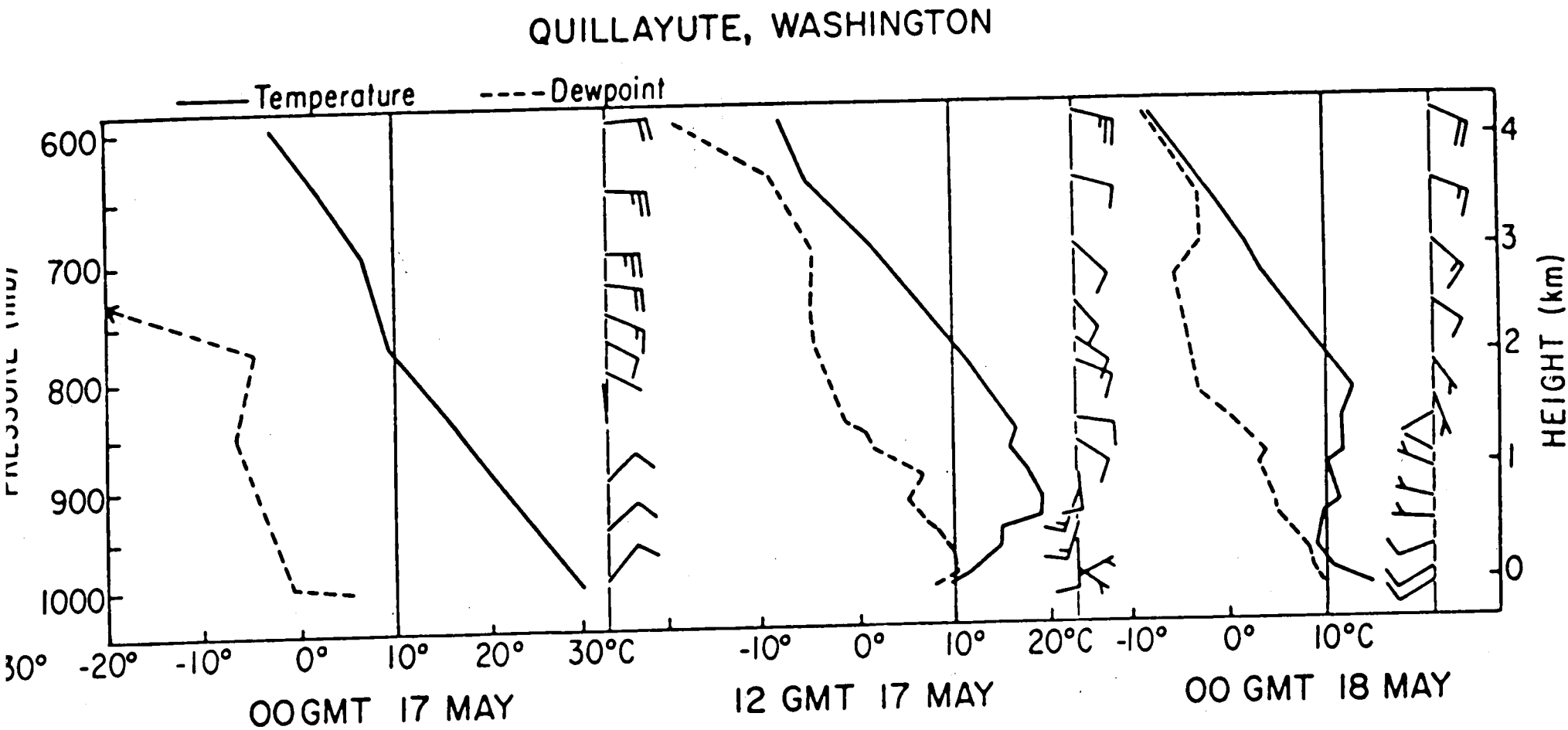

FIG. 21. Vertical soundings at Quillayute, WA before (00 UTC 17 May) and after (12 UTC 17 May, 00 JTC 18 May) the passage of the alongshore surge at that location. Winds are plotted to the right of the ppropriate temperature sounding.